



MAX-PLANCK-INSTITUT  
FÜR PLASMAPHYSIK

## Research Internship (PRe)

**Major:** Applied Mathematics  
**School year:** 2024-2025

Contribution to the development of Psydac, a finite element library.

Implementation of solid mechanics equations using Psydac and simulation on a supercomputer.

**Non-confidential report and Can be published on the Internet**

**Author :** Arasu Candassamy

**Year Group:** 2026

**ENSTA Supervisor:**

SONIA FLISS  
sonia.fliss@ensta.fr

**Host Organization Supervisor:**

MARTIN CAMPOS-PINTO  
martin.campos-pinto@ipp.mpg.de

**Internship from 26/05/2025 to 22/08/2025**

**Name of the host organization:** Max-Planck-Institute Für Plasmaphysik  
**Address:** Boltzmannstrasse 2, 85748 Garching bei München



## Abstract

Lorem ipsum dolor sit amet, consectetuer adipiscing elit. Ut purus elit, vestibulum ut, placerat ac, adipiscing vitae, felis. Curabitur dictum gravida mauris. Nam arcu libero, nonummy eget, consectetuer id, vulputate a, magna. Donec vehicula augue eu neque. Pellentesque habitant morbi tristique senectus et netus et malesuada fames ac turpis egestas. Mauris ut leo. Cras viverra metus rhoncus sem. Nulla et lectus vestibulum urna fringilla ultrices. Phasellus eu tellus sit amet tortor gravida placerat. Integer sapien est, iaculis in, pretium quis, viverra ac, nunc. Praesent eget sem vel leo ultrices bibendum. Aenean faucibus. Morbi dolor nulla, malesuada eu, pulvinar at, mollis ac, nulla. Curabitur auctor semper nulla. Donec varius orci eget risus. Duis nibh mi, congue eu, accumsan eleifend, sagittis quis, diam. Duis eget orci sit amet orci dignissim rutrum.

Nam dui ligula, fringilla a, euismod sodales, sollicitudin vel, wisi. Morbi auctor lorem non justo. Nam lacus libero, pretium at, lobortis vitae, ultricies et, tellus. Donec aliquet, tortor sed accumsan bibendum, erat ligula aliquet magna, vitae ornare odio metus a mi. Morbi ac orci et nisl hendrerit mollis. Suspendisse ut massa. Cras nec ante. Pellentesque a nulla. Cum sociis natoque penatibus et magnis dis parturient montes, nascetur ridiculus mus. Aliquam tincidunt urna. Nulla ullamcorper vestibulum turpis. Pellentesque cursus luctus mauris.

Keywords:

## Résumé

Lorem ipsum dolor sit amet, consectetuer adipiscing elit. Ut purus elit, vestibulum ut, placerat ac, adipiscing vitae, felis. Curabitur dictum gravida mauris. Nam arcu libero, nonummy eget, consectetuer id, vulputate a, magna. Donec vehicula augue eu neque. Pellentesque habitant morbi tristique senectus et netus et malesuada fames ac turpis egestas. Mauris ut leo. Cras viverra metus rhoncus sem. Nulla et lectus vestibulum urna fringilla ultrices. Phasellus eu tellus sit amet tortor gravida placerat. Integer sapien est, iaculis in, pretium quis, viverra ac, nunc. Praesent eget sem vel leo ultrices bibendum. Aenean faucibus. Morbi dolor nulla, malesuada eu, pulvinar at, mollis ac, nulla. Curabitur auctor semper nulla. Donec varius orci eget risus. Duis nibh mi, congue eu, accumsan eleifend, sagittis quis, diam. Duis eget orci sit amet orci dignissim rutrum.

Nam dui ligula, fringilla a, euismod sodales, sollicitudin vel, wisi. Morbi auctor lorem non justo. Nam lacus libero, pretium at, lobortis vitae, ultricies et, tellus. Donec aliquet, tortor sed accumsan bibendum, erat ligula aliquet magna, vitae ornare odio metus a mi. Morbi ac orci et nisl hendrerit mollis. Suspendisse ut massa. Cras nec ante. Pellentesque a nulla. Cum sociis natoque penatibus et magnis dis parturient montes, nascetur ridiculus mus. Aliquam tincidunt urna. Nulla ullamcorper vestibulum turpis. Pellentesque cursus luctus mauris.

Mots-clés:



## Acknowledgement

Lorem ipsum dolor sit amet, consectetuer adipiscing elit. Ut purus elit, vestibulum ut, placerat ac, adipiscing vitae, felis. Curabitur dictum gravida mauris. Nam arcu libero, nonummy eget, consectetuer id, vulputate a, magna. Donec vehicula augue eu neque. Pellentesque habitant morbi tristique senectus et netus et malesuada fames ac turpis egestas. Mauris ut leo. Cras viverra metus rhoncus sem. Nulla et lectus vestibulum urna fringilla ultrices. Phasellus eu tellus sit amet tortor gravida placerat. Integer sapien est, iaculis in, pretium quis, viverra ac, nunc. Praesent eget sem vel leo ultrices bibendum. Aenean faucibus. Morbi dolor nulla, malesuada eu, pulvinar at, mollis ac, nulla. Curabitur auctor semper nulla. Donec varius orci eget risus. Duis nibh mi, congue eu, accumsan eleifend, sagittis quis, diam. Duis eget orci sit amet orci dignissim rutrum.

Nam dui ligula, fringilla a, euismod sodales, sollicitudin vel, wisi. Morbi auctor lorem non justo. Nam lacus libero, pretium at, lobortis vitae, ultricies et, tellus. Donec aliquet, tortor sed accumsan bibendum, erat ligula aliquet magna, vitae ornare odio metus a mi. Morbi ac orci et nisl hendrerit mollis. Suspendisse ut massa. Cras nec ante. Pellentesque a nulla. Cum sociis natoque penatibus et magnis dis parturient montes, nascetur ridiculus mus. Aliquam tincidunt urna. Nulla ullamcorper vestibulum turpis. Pellentesque cursus luctus mauris.

---

# Contents

<b>Abstract</b>	<b>3</b>
<b>Acknowledgement</b>	<b>5</b>
<b>1 Introduction</b>	<b>7</b>
<b>2 Linear Elasticity</b>	<b>8</b>
2.1 Physical Model and Strong Formulation . . . . .	8
2.2 Pure displacement weak-formulation . . . . .	9
2.3 Numerical simulation using PSYDAC on the Supercomputer Raven . . . . .	11
2.3.1 Dirichlet Homogeneous Boundary conditions on $\partial\Omega_D = \partial\Omega$ . . . . .	12
2.3.2 Mixed boundary conditions . . . . .	15
2.4 Mixed displacement-pressure formulation . . . . .	19
2.4.1 Well-posedness of the mixed displacement-pressure formulation . . . . .	20
2.4.2 Isogeometric discretisation and a priori error estimate . . . . .	21
2.4.3 Example of simulation using PSYDAC . . . . .	22
<b>3 Thermoelasticity</b>	<b>24</b>
3.1 Introduction . . . . .	24
3.2 Simplified problem - Physical model and equations . . . . .	24
3.2.1 Problem setup and parameters . . . . .	24
3.2.2 Strong Formulation . . . . .	25
3.2.3 Weak Formulation . . . . .	27
3.2.4 Numerical simulation . . . . .	28
<b>4 References</b>	<b>32</b>
<b>5 Appendices</b>	<b>34</b>
5.1 Other plots of solutions for the problem with Dirichlet Homogeneous Boundary Conditions . . . . .	34

# Chapter 1

## Introduction

The Max-Planck Institute for Plasma Physics (IPP), located in Garching and Greifswald, is a renowned research institute in Plasma physics and Nuclear fusion. Founded under the Max-Planck Society in 1960, this institute has a long tradition of scientific excellence and innovation. The Department of Numerical Methods for Plasma Physics (NMPP), where my internship took place, plays a crucial role in developing advanced simulation techniques to understand and predict the behavior of plasmas in complex environments (in tokamaks or stelarators).

The Finite Element Method (FEM) is a widely used numerical technique for solving Partial Differential Equations (PDEs). It is particularly well-suited for addressing plasma physics problems due to its ability to handle complex geometries and varied boundary conditions. FEM allows for the discretization of a continuous domain into a set of finite elements, thereby facilitating the numerical resolution of equations governing the physical phenomena under study.

In the context of electromagnetism, the Finite Element Exterior Calculus (FEEC) formulation is a powerful approach for solving Maxwell's equations. This method is particularly suitable for problems involving electromagnetic fields, as it preserves certain topological and physical properties of the original equations. FEEC provides a powerfull framework for plasma simulation, where electromagnetic interactions play a central role.

Psydac is an integrated development environment (IDE) specifically designed for simulation and data analysis in plasma physics. It offers a range of tools to facilitate the implementation of numerical methods, including FEM and FEEC frameworks. Psydac enables researchers to develop complex models, simulate them, and analyze results efficiently and intuitively. Psydac also stands out as an isogeometric analysis library, an approach that integrates geometric modeling and numerical analysis within a unified framework. Isogeometric analysis allows simulations to be performed directly on the geometric models used for design, eliminating the need to convert CAD models into traditional meshes for simulations. This provides increased accuracy and better integration between design and analysis, reducing errors and improving the efficiency of the simulation process. Using Psydac, researchers can leverage these capabilities to develop more accurate models and perform more reliable analyses, which is particularly advantageous in the complex field of plasma physics.

This internship report describes my experience and contributions within the NMPP Department at the IPP. Psydac should be able to solve any PDEs but it hasn't been tested on equations from solid mechanics. Then, during this internship, I have explored the linear elasticity problem, its simulation using Psydac and its running on Supercomputer Raven.

# Chapter 2

## Linear Elasticity

### 2.1 Physical Model and Strong Formulation

The following presentation of the context of work and physical background comes from [Gou13] and [EG04]. Let's denote by  $\Omega \subset \mathbb{R}^3$  a deformable medium characterized by  $\lambda$  and  $\mu$  Lamé's coefficient ( $\lambda, \mu > 0$ ).  $\Omega$  is a bounded open domain with lipschitzian boundary.  $\lambda$  is called Lamé's first coefficient,  $\mu$  is the shear modulus. These coefficient are related to the Young modulus and Poisson coefficient of the medium. The deformable medium is under an external load  $\vec{f} : \Omega \rightarrow \mathbb{R}^3$ . Then, we are looking for  $\vec{u} : \Omega \rightarrow \mathbb{R}^3$  the displacement field, when the equilibrium is reached.

The material verifies the following equilibrium condition :

$$\nabla \cdot \boldsymbol{\sigma}(\vec{u}) + \vec{f} = \vec{0} \text{ in } \Omega, \quad (2.1)$$

where  $\boldsymbol{\sigma}(\vec{u})$  is the Cauchy Stress Tensor, defined by  $\boldsymbol{\sigma}(\vec{u}) = C : \boldsymbol{\varepsilon}(\vec{u})$ .  $C$  is the fourth-order stiffness tensor and  $\boldsymbol{\varepsilon}(\vec{u}) := \frac{1}{2}(\nabla \vec{u} + (\nabla \vec{u})^T)$  is the strain tensor. In the context of linear elasticity, the relation between  $\boldsymbol{\varepsilon}(\vec{u})$  and  $\boldsymbol{\sigma}(\vec{u})$  is simpler :

$$\boldsymbol{\sigma}(\vec{u}) = \lambda \operatorname{Tr}(\boldsymbol{\varepsilon}) I_3 + 2\mu \boldsymbol{\varepsilon} = \lambda(\nabla \cdot \vec{u}) I_3 + \mu(\nabla \vec{u} + (\nabla \vec{u})^T) \text{ in } \Omega. \quad (2.2)$$

For boundary conditions, there are two types of boundary conditions : Dirichlet conditions on the displacement field  $\vec{u}$  and Traction conditions on the Cauchy Stress Tensor  $\boldsymbol{\sigma}(\vec{u})$ .

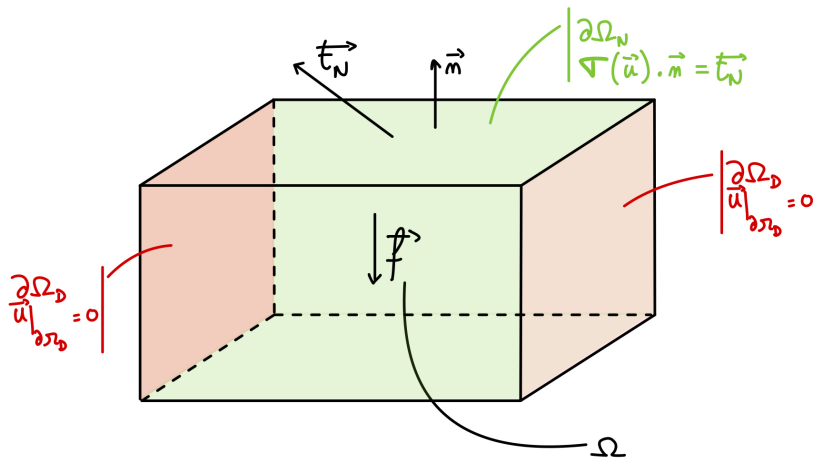


Figure 2.1: Representation of a domain  $\Omega$

Let's decompose  $\partial\Omega$  as  $\partial\Omega_D$  and  $\partial\Omega_N$  such that  $\partial\Omega_D \cup \partial\Omega_N = \partial\Omega$ ,  $\partial\Omega_D \cap \partial\Omega_N = \emptyset$ . Let's denote by  $\vec{t}_N : \partial\Omega_N \rightarrow \mathbb{R}^3$  the normal traction force and  $\vec{n}$  the normal vector of  $\partial\Omega$  outside-oriented. We can consider the boundary displacement on  $\partial\Omega_D$  as equal to  $\vec{0}$ .

In case of non-homogenous boundary conditions  $\vec{g} : \partial\Omega_D \rightarrow \mathbb{R}^3$ , we can solve the problem for  $\vec{u} - \vec{g}$  by modifying the source term. Then, the solution of linear elasticity problem should verify :

$$\begin{cases} \vec{u} = \vec{0} & \partial\Omega_D \\ \boldsymbol{\sigma}(\vec{u}) \cdot \vec{n} = \vec{t}_N & \partial\Omega_N \end{cases}$$

Physically,  $\vec{f}$  is a "volume force" on  $\Omega$  and  $\vec{t}_N$  is a "surface force". The strong formulation of this problem is :

For a given  $\vec{f} \in \mathbf{L}^2(\Omega)$ ,  $\vec{t}_N \in \mathbf{L}^2(\partial\Omega_N)$ , find  $\vec{u} \in \mathbf{H}^1(\Omega)$  such that :

$$\begin{cases} -\nabla \cdot \boldsymbol{\sigma}(\vec{u}) = \vec{f} & \text{in } \Omega \quad (\text{Equilibrium}) \\ \boldsymbol{\sigma}(\vec{u}) = \lambda(\nabla \cdot \vec{u})I_3 + \mu(\nabla \vec{u} + (\nabla \vec{u})^T) & \text{in } \Omega \quad (\text{Hook's law}) \\ \vec{u} = \vec{0} & \text{in } \partial\Omega_D \\ \boldsymbol{\sigma}(\vec{u}) \cdot \vec{n} = \vec{t}_N & \text{in } \partial\Omega_N \end{cases} \quad (2.3)$$

where  $\mathbf{L}^2(\Omega) = (L^2(\Omega))^3$ ,  $\mathbf{L}^2(\partial\Omega_N) = (L^2(\partial\Omega_N))^3$ ,  $\mathbf{H}^1(\Omega) = (H^1(\Omega))^3$ ,

## 2.2 Pure displacement weak-formulation

To derive the weak formulation from (2.3), let's introduce the following functionnal space :  $\mathbf{H}_{0,D}^1(\Omega) = \left\{ \vec{v} \in \mathbf{H}^1(\Omega) \mid \vec{v}|_{\partial\Omega_D} = \vec{0} \right\}$ , which is a sub-hilbert space of  $\mathbf{H}^1(\Omega)$  equipped with the same dot product (as a closed space of a Hilbert space). By taking the scalar product of the equilibrium equation from (2.3) with  $\vec{v} \in (H_{0,D}^1(\Omega))^3$  and applying a Green's formula, one gets that :

$$\int_{\Omega} \boldsymbol{\sigma}(\vec{u}) : (\nabla \vec{v}) dV - \int_{\partial\Omega} (\boldsymbol{\sigma}(\vec{u}) \cdot \vec{n}) \cdot \vec{v} dS = \int_{\Omega} \vec{f} \cdot \vec{v} dV$$

One can remark that with (2.2), the tensor  $\boldsymbol{\sigma}(\vec{u})$  is symetric. It implies that :  $\boldsymbol{\sigma}(\vec{u}) : \nabla \vec{v} = \boldsymbol{\sigma}(\vec{u}) : \boldsymbol{\epsilon}(\vec{v})$ . Moreover,  $\vec{v} \in (H_{0,D}^1(\Omega))^3$ , then  $\vec{v}|_{\partial\Omega_D} = \vec{0}$ . So the weak formulation can be simplified into :

$$\begin{cases} \text{Find } \vec{u} \in \mathbf{H}_{0,D}^1(\Omega) \text{ such that :} \\ a(\vec{u}, \vec{v}) = l(\vec{v}) \quad \forall \vec{v} \in \mathbf{H}_{0,D}^1(\Omega) \end{cases} \quad (2.4)$$

With :

$$a : \begin{cases} \mathbf{H}_{0,D}^1(\Omega) \times \mathbf{H}_{0,D}^1(\Omega) \rightarrow \mathbb{R} \\ (\vec{u}, \vec{v}) \mapsto \int_{\Omega} \boldsymbol{\sigma}(\vec{u}) : \boldsymbol{\epsilon}(\vec{v}) dV = \int_{\Omega} \lambda(\nabla \cdot \vec{u})(\nabla \cdot \vec{v}) dV + \int_{\Omega} 2\mu \boldsymbol{\epsilon}(\vec{u}) : \boldsymbol{\epsilon}(\vec{v}) dV \end{cases}$$

$$l : \begin{cases} \mathbf{H}_{0,D}^1(\Omega) \rightarrow \mathbb{R} \\ \vec{v} \mapsto \int_{\Omega} \vec{f} \cdot \vec{v} dV + \int_{\partial\Omega_N} \vec{t}_N \cdot \vec{v} dS \end{cases}$$

In continuum mechanics, (2.4) is called the Principle of Virtual Work. Let's look at the well-posedness of (2.4). Before starting, let's remind some notations and lemmas.

$\|\cdot\|_{\mathbf{H}^1(\Omega)}$  is defined as :  $\forall \vec{v} \in \mathbf{H}^1(\Omega)$ ,  $\|\vec{v}\|_{\mathbf{H}^1(\Omega)} = \left( \sum_{i=1}^3 \|v_i\|_{H^1(\Omega)} \right)^{1/2}$ .

**Lemma 2.2.1.** 1.  $\forall \vec{u} \in \mathbf{H}^1(\Omega)$ ,  $\int_{\Omega} (\nabla \cdot \vec{u})^2 dV \leq 3 \|\vec{u}\|_{\mathbf{H}^1(\Omega)}^2$

2.  $\forall \vec{u} \in \mathbf{H}^1(\Omega)$ ,  $\boldsymbol{\epsilon}(\vec{u}) : \boldsymbol{\epsilon}(\vec{u}) \leq \nabla \vec{u} : \nabla \vec{u}$ . Then :  $\int_{\Omega} \boldsymbol{\epsilon}(\vec{u}) : \boldsymbol{\epsilon}(\vec{u}) d\Omega \leq \int_{\Omega} \nabla \vec{u} : \nabla \vec{u} d\Omega \leq \|\vec{u}\|_{\mathbf{H}^1(\Omega)}^2$

*Proof.* By calculus, or a detailed version in [Cin18] □

**Lemma 2.2.2.** (*First Korn's inequality*)

Let  $\Omega \subset \mathbb{R}^3$  a domain and denotes by  $\|\boldsymbol{\varepsilon}(\vec{u})\|_{\mathbf{L}^2(\Omega)} := (\int_{\Omega} \boldsymbol{\varepsilon}(\vec{u}) : \boldsymbol{\varepsilon}(\vec{u}))^{1/2}$ . Then, there exists  $C > 0$  such that:  $\forall \vec{v} \in \mathbf{H}_{\vec{0}}^1(\Omega)$ ,  $C\|\vec{v}\|_{\mathbf{H}^1(\Omega)} \leq \|\boldsymbol{\varepsilon}(\vec{v})\|_{\mathbf{L}^2(\Omega)}$

*Proof.* A proof can be found in [BS08] □

**Lemma 2.2.3.** (*Second Korn's inequality*)

Let  $\Omega \subset \mathbb{R}^3$  a domain. Then, there exists  $C > 0$  such that:  $\forall \vec{v} \in \mathbf{H}^1(\Omega)$ ,  $C\|\vec{v}\|_{\mathbf{H}^1(\Omega)} \leq \|\boldsymbol{\varepsilon}(\vec{v})\|_{\mathbf{L}^2(\Omega)} + \|\vec{v}\|_{\mathbf{L}^2(\Omega)}$ . By Rellich theorem,  $\mathbf{H}^1(\Omega)$  is compactly embedded in  $\mathbf{L}^2(\Omega)$  as  $\Omega$  is a open bounded domain. Then, one can show that there exists  $C > 0$  such that:  $\forall \vec{v} \in \mathbf{H}^1(\Omega)$ ,  $C\|\vec{v}\|_{\mathbf{H}^1(\Omega)} \leq \|\boldsymbol{\varepsilon}(\vec{v})\|_{\mathbf{L}^2(\Omega)}$

*Proof.* A proof can be found in [BS08] □

Now, we can prove the well-posedness of (2.4) when  $|\Omega_D| > 0$ .

- $(\mathbf{H}_{\vec{0},D}^1(\Omega), \|\cdot\|_{\mathbf{H}^1(\Omega)})$  is a Hilbert space.
- $a(\cdot, \cdot)$  is a bilinear form on  $\mathbf{H}_{\vec{0},D}^1(\Omega) \times \mathbf{H}_{\vec{0},D}^1(\Omega)$  and  $l(\cdot)$  a linear form on  $\mathbf{H}_{\vec{0},D}^1(\Omega)$ .
- $l(\cdot)$  is continuous :

$$\begin{aligned} \forall \vec{v} \in \mathbf{H}_{\vec{0},D}^1(\Omega), |l(\vec{v})| &\leq \left| \left( \vec{f}, \vec{v} \right)_{\mathbf{L}^2(\Omega)} + \left( \vec{t}_N, \vec{v} \right)_{\mathbf{L}^2(\partial\Omega_N)} \right| \\ |l(\vec{v})| &\leq \left( \|\vec{f}\|_{\mathbf{L}^2(\Omega)} + \|\gamma_0\| \|\vec{t}_N\|_{\mathbf{L}^2(\partial\Omega_N)} \right) \|\vec{v}\|_{\mathbf{H}^1(\Omega)} \end{aligned}$$

- $a(\cdot, \cdot)$  is continuous:

$$\forall \vec{u}, \vec{v} \in \mathbf{H}_{\vec{0},D}^1(\Omega), |a(\vec{u}, \vec{v})| \leq |a(\vec{u}, \vec{u})|^{1/2} |a(\vec{v}, \vec{v})|^{1/2} \quad \text{By Cauchy-Schwarz Inequality as } a(\cdot, \cdot) \text{ is a symmetric and positive bilinear form}$$

$$|a(\vec{u}, \vec{v})| \leq (3\lambda + 2\mu) \|\vec{u}\|_{\mathbf{H}^1(\Omega)} \|\vec{v}\|_{\mathbf{H}^1(\Omega)}.$$

- $a(\cdot, \cdot)$  is coercive:

- If  $\Omega_D = \Omega$ , then  $\mathbf{H}_{\vec{0},D}^1(\Omega) = \mathbf{H}_{\vec{0}}^1(\Omega)$  and we can apply **Lemma 2.2.2** : there exists  $C > 0$  such that:

$$\begin{aligned} \forall \vec{u} \in \mathbf{H}_{\vec{0},D}^1(\Omega), \quad a(u, u) &= \int_{\Omega} \lambda(\boldsymbol{\nabla} \cdot \vec{u})^2 dV + \int_{\Omega} 2\mu \boldsymbol{\varepsilon}(\vec{u}) : \boldsymbol{\varepsilon}(\vec{u}) dV \\ &\geq 2\mu \|\boldsymbol{\varepsilon}(\vec{u})\|_{\mathbf{L}^2(\Omega)} \\ a(u, u) &\geq 2\mu C \|\vec{u}\|_{\mathbf{H}^1(\Omega)}^2 \end{aligned}$$

- If  $\Omega_D \subsetneq \Omega$ , we can now apply **Lemma 2.2.3** : there exists  $C > 0$  such that:  $\forall \vec{u} \in \mathbf{H}_{\vec{0},D}^1(\Omega)$ ,  $a(u, u) \geq 2\mu C \|\vec{u}\|_{\mathbf{H}^1(\Omega)}$

Then, by Lax-Milgram theorem, the problem (2.4) is well-posed when  $|\Omega_D| > 0$ . When,  $|\Omega_D| = 0$ , (2.4) turns into the **Pure Traction Problem** :

$$\begin{cases} \text{Find } \vec{u} \in \mathbf{H}^1(\Omega) \text{ such that :} \\ a(\vec{u}, \vec{v}) = \int_{\Omega} \vec{f} \cdot \vec{v} dV + \int_{\partial\Omega} \vec{t}_N \cdot \vec{v} dS =: l(\vec{v}) \quad \forall \vec{v} \in \mathbf{H}^1(\Omega) \end{cases} \quad (2.5)$$

This problem isn't really well-posed. Regarding to the Rigid Displacement Field (translations and rotations)  $\mathcal{R} = \left\{ \vec{v} \in \mathbf{H}^1(\Omega) \mid \exists x_1, x_2 \in \mathbb{R}^3, \vec{v}(x) = x_1 + x_2 \times x \right\}, \forall \vec{v} \in \mathcal{R}, \nabla \cdot v = 0 \text{ and } \boldsymbol{\epsilon}(\vec{v}) = 0.$ . Then :  $\forall \vec{u} \in \mathbf{H}^1(\Omega), \forall \vec{v} \in \mathcal{R}, a(\vec{u}, \vec{v}) = 0.$  So, the weak formulation (2.5) is solvable iff the following compatibility equality holds :  $\forall \vec{v} \in \mathcal{R}, \int_{\Omega} \vec{f} \cdot \vec{v} dV + \int_{\partial\Omega} \vec{t}_N \cdot \vec{v} dS = 0,$  and in this case, there exists an unique solution  $\vec{u} \in \hat{\mathbf{H}}^1(\Omega) := \left\{ \vec{v} \in \mathbf{H}^1(\Omega) \mid \int_{\Omega} \vec{v} dV = \int_{\Omega} \nabla \times \vec{v} dV = \vec{0} \right\}$  In case of **Pure Traction Problem**, we are looking for a solution modulo a rigid displacement field. *A more rigorous proof of the equivalence can be found in [BS08] and [Che24].*

## 2.3 Numerical simulation using PSYDAC on the Supercomputer Raven

PSYDAC is high-level programming IDE and very intuitive to use. It is using SymPDE and Pyccel. SymPDE implements in Python abstract objects (Functionnal Space, differential operators, linear and bilinear forms...). Pyccel is a transpiler, used to convert a Python Code into a C or Fortran code, in order to take advantage from code acceleration and parallelization. The figure 2.2 summarize the dependancy between PSYDAC, SymPDE and Pyccel. A more detailed presentation of PSYDAC can be found in [GHR22].

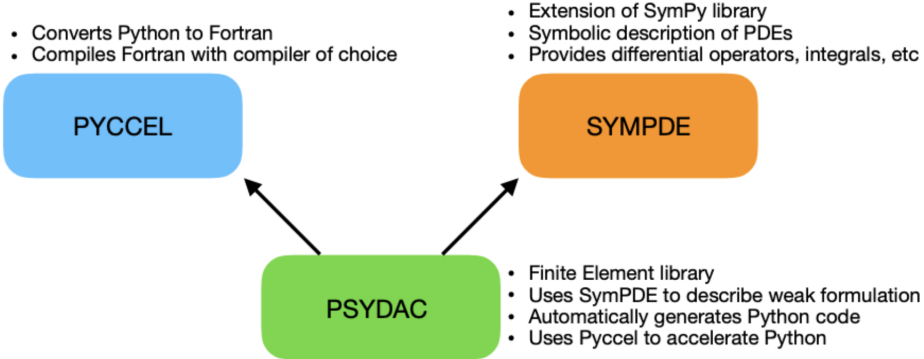


Figure 2.2: Dependancy graph of PSYDAC, from [GHR22]

Raven is a supercomputer located at the Max-Planck Institute for Plasma Physics. It is part of the High Performance Computing (HPC) infrastructure and is used for large-scale simulations and data analysis in plasma physics and related fields. I had the opportunity to run my simulations on Raven, which provided me with access to powerful computational resources and parallel processing capabilities.

### 2.3.1 Dirichlet Homogeneous Boundary conditions on $\partial\Omega_D = \partial\Omega$

In a first time, to get the grips with PSYDAC and the HPC, I have considered the case  $\Omega = [0, 1]^3$ ,  $\partial\Omega_D = \partial\Omega$  and  $\partial\Omega_N = \emptyset$ . To verify if the numerical resolution of PSYDAC of (2.4) is correct, I have used the Method of Manufactured Solutions. The concept is quite simpler, we assume that a function  $\vec{u}_e \in \mathbf{H}_0^1(\Omega)$  verifies the strong problem (2.3), then we compute the source term  $\vec{f}$  and we solve the (2.4) with  $\vec{f}$  as a source term and we look at the error between the numerical solution and the

theoretical one. I have considered  $\vec{u}_e$  defined as :  $\vec{u}_e = \begin{pmatrix} 0 \\ 0 \\ \sin(\pi x) \sin(\pi y) \sin(\pi z) \end{pmatrix} \in \mathbf{H}_0^1(\Omega)$ . Then,

we can compute manually the source term  $\vec{f}$  :  $\vec{f} = \begin{pmatrix} -\pi^2(\lambda + \mu) \cos(\pi x) \sin(\pi y) \cos(\pi z) \\ -\pi^2(\lambda + \mu) \sin(\pi x) \cos(\pi y) \cos(\pi z) \\ \pi^2(\lambda + 4\mu) \sin(\pi x) \sin(\pi y) \sin(\pi z) \end{pmatrix} \in \mathbf{L}^2(\Omega)$ .

To make the numerical simulation with PSYDAC, we have to choose two important parameters :  $d$  the maximum degree of B-Splines functions that will approximate the solution and  $n_{\text{cells}}$  is the number of cells in each dimension of  $\Omega$  for the finite dimensional space.  $h \propto \frac{1}{n_{\text{cells}}}$ , an usual discretization parameters for finite dimensional spaces and  $d$  will conduct the convergence speed of the numerical solution. By solving the problem Dirichlet Homogeneous Boundary conditions on the whole border, one can observe the following plots of the simulated  $\vec{u}_{e,3}^h$  for different plane  $z$ . It is possible to plot also the error  $\vec{u}_{e,3} - \vec{u}_{e,3}^h$ .

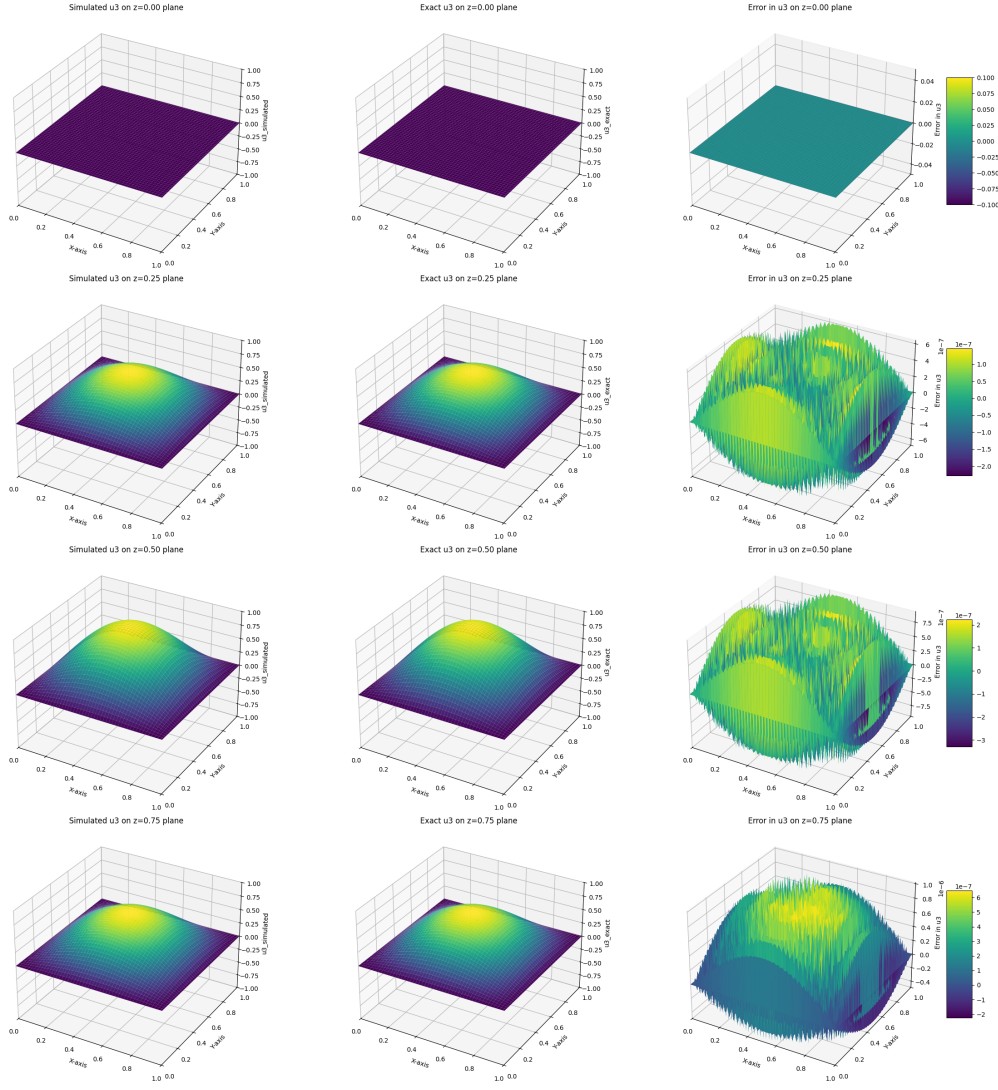


Figure 2.3: Plots comparison between the simulated and real  $u_{e,3}$  with the error, for different plane  $z$ , with  $d = 2$  and  $n_{\text{cell}} = 64$

We can observe that the numerical solution is "quite" near the real solution. To get a better estimation of convergence rate, let's look at the Céa's lemma in this case.

Denotes by  $\mathbf{V}^h \subset \mathbf{H}^1(\Omega)$  the discrete finite dimensional space,  $\vec{u} \in \mathbf{H}^{s+1}(\Omega) \subset \mathbf{H}^1(\Omega)$ ,  $1 \leq s \leq d + 1$  the real solution solution and  $\vec{u}^h \in \mathbf{V}^h$  the discrete solution. Then, the Céa's lemma gives the following estimates :  $\|\vec{u} - \vec{u}^h\|_{\mathbf{H}^1(\Omega)} \leq \frac{3\lambda+2\mu}{2\mu C} \inf_{\vec{v}^h \in \mathbf{H}^1(\Omega)} \|\vec{u} - \vec{v}^h\|_{\mathbf{H}^1(\Omega)}$  where  $C > 0$  is a constant from Korn's inequality (independant of  $h$ ). By applying **Corollary 4.21, 4.27, Theorem 6.2** from [DV+14] and Aubin-Nitsche theorem, we can get the following estimates :

$$\begin{aligned} \|\vec{u} - \vec{u}^h\|_{\mathbf{H}^1(\Omega)} &\lesssim \frac{3\lambda + 2\mu}{2\mu C} h^q \|\vec{u}\|_{\mathbf{H}^{q+1}(\Omega)} \\ \|\vec{u} - \vec{u}^h\|_{L^2(\Omega)} &\lesssim (3\lambda + 2\mu) h^{q+1} \|\vec{u}\|_{\mathbf{H}^{q+1}(\Omega)} \end{aligned} \quad (2.6)$$

where  $q = \min(s, d)$ . In this case,  $u_e$  is an infinitely smooth solution, then  $q = d$ .

We can see that the numerical solution converges with the expected order to the real solution : the more the mesh is refined, the more the error is lower and the more the splines' degree is higher, the more the convergence rate is higher. For this numerical resolution, I have used **GMRES** method to solve the linear system at the end of the discretization. That needed to take care of the tolerance of the solver, because with a fixed tolerance, if the  $d$  and  $n_{\text{cells}}$  are "too higher", the convergence rate

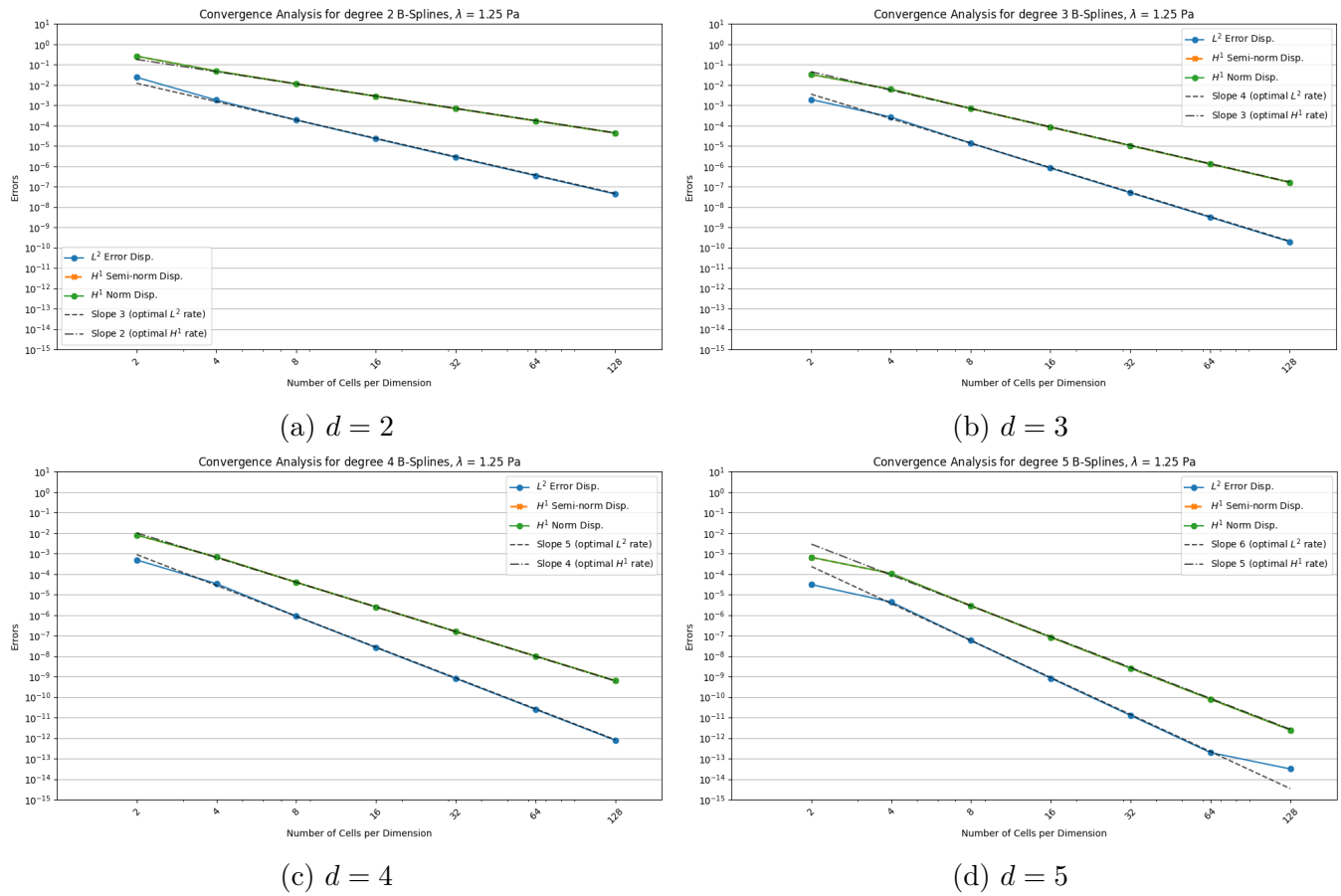


Figure 2.4: Four plots of relative errors ( $\|\vec{u} - \vec{u}^h\|_{H^1(\Omega)}$  and  $\|\vec{u} - \vec{u}^h\|_{L^2(\Omega)}$ ) with different degree B-Splines (with  $\lambda = 1.25$  and  $\mu = 1$ )

cannot hold. The following figure illustrates this case, when  $d = 5$  and  $n_{\text{cells}} = 16$ .

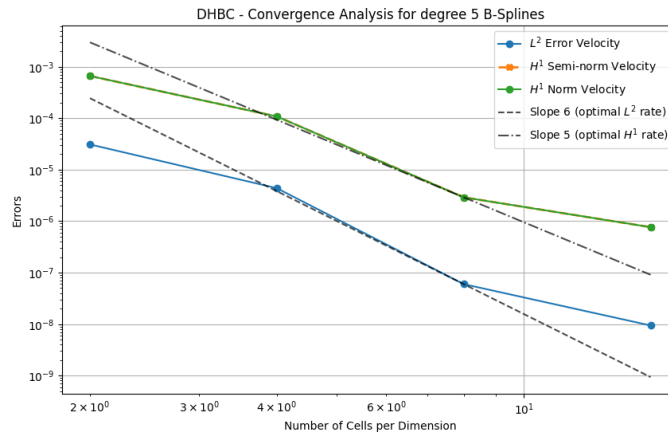


Figure 2.5: Error plot between exact and numerical solution with degree 5 B-Splines with "higher" tolerance for the solver

But even with a lower tolerance for the solver ( $10^{-15}$  for figure 2.4d), the error reaches a plateau, which is not the case for lower degree B-Splines (at least for the tested configurations). This plateau can be explained by the matrix of the bilinear form  $a(.,.)$  which is ill-conditioned. Moreover, the bad conditioning can become worse with more refined mesh and higher degree B-Splines (as the convergence is faster).

### 2.3.2 Mixed boundary conditions

Then, I have made a simulation with Mixed Boundary Conditions, as it is introduced in (2.3), with also non-homogeneous Dirichlet boundary conditions.

Again,  $\Omega = [0, 1]^3$ , with :

$$\partial\Omega_{DH} = \{(x, y, z) \in \partial\Omega \mid z = 0 \text{ or } z = 1\} \quad \partial\Omega_{DNH} = \{(x, y, z) \in \partial\Omega \mid x = 0 \text{ or } x = 1\}$$

$$\partial\Omega_N = \{(x, y, z) \in \partial\Omega \mid y = 0 \text{ or } y = 1\}$$

For that purpose,  $\vec{u}_e$ ,  $\vec{f}$ ,  $\vec{t}_N$  and  $\vec{g}$  are now defined as :

$$\vec{u}_e = \begin{pmatrix} 0 \\ 0 \\ \sin(\pi z) \cos(\pi x) \cos(\pi y) \end{pmatrix}, \vec{f} = \begin{pmatrix} \pi^2 (\lambda + \mu) \sin(\pi x) \cos(\pi y) \cos(\pi z) \\ \pi^2 (\lambda + \mu) \sin(\pi y) \cos(\pi x) \cos(\pi z) \\ \pi^2 (\lambda + 4\mu) \sin(\pi z) \cos(\pi x) \cos(\pi y) \end{pmatrix}$$

$$\vec{t}_N = \begin{pmatrix} 0 \\ -\lambda \pi \cos(\pi x) \cos(\pi z) \\ 0 \end{pmatrix}, \vec{g} = \begin{pmatrix} 0 \\ 0 \\ \pm \sin(\pi z) \cos(\pi y) \end{pmatrix}$$

Then, we can get the same plots and interpretation as before.

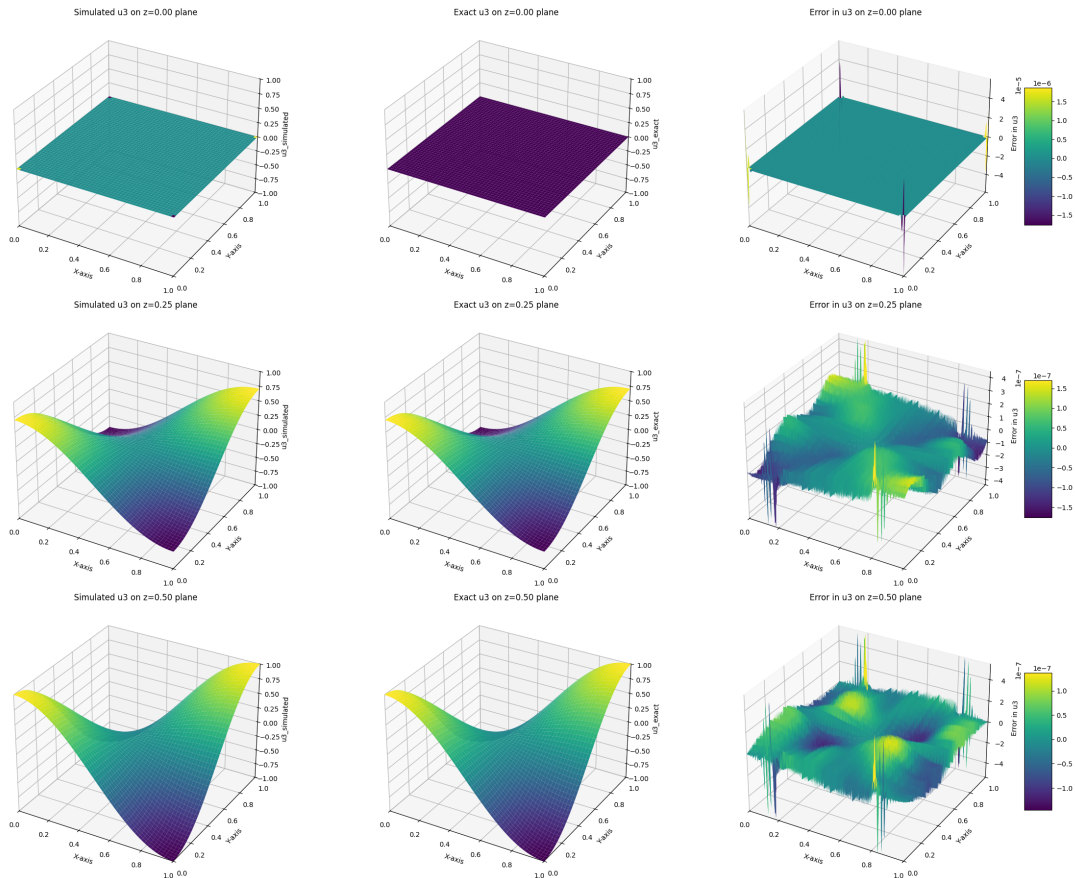


Figure 2.6: Plots comparison between the simulated and real  $u_{e,3}$  with the error, for different plane  $z$ , with  $d = 2$  and  $n_{\text{cell}} = 128$

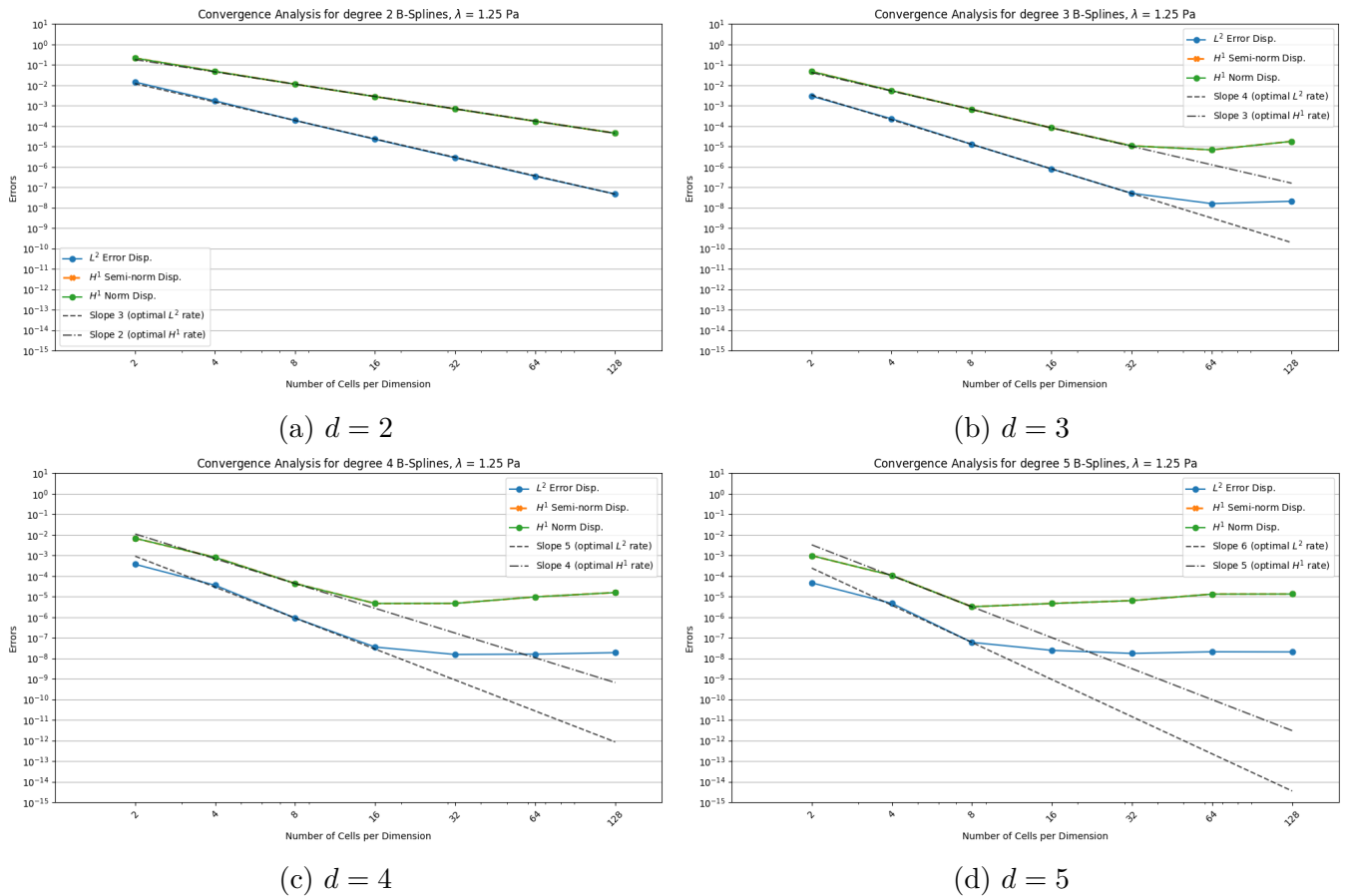


Figure 2.7: Four plots of relative errors ( $\|\vec{u} - \vec{u}^h\|_{H^1(\Omega)}$  and  $\|\vec{u} - \vec{u}^h\|_{L^2(\Omega)}$ ) with different degree B-Splines (with  $\lambda = 1.25$  and  $\mu = 1$ )

For fixed value  $\lambda = 1.25$  and  $\mu = 1$ , the codes seems to give a numerical solution that converges to the theoretical one with the expected order. We can notice that the plateau effect comes back and appears faster than in the case of Dirichlet Homogeneous Boundary Conditions. The  $L^2$  error seems to converge to a value slightly higher than  $10^{-8}$ , while the  $H^1$  error converges to a value slightly higher than  $10^{-5}$ , and this phenomena is more pronounced for higher degree B-Splines. The limit value of each error seems to be the same for all degree B-Splines, when the  $L^2$  error becomes lower than  $10^{-7}$  and the  $H^1$  error becomes lower than  $10^{-5}$ . So, this plateau effect is not due to the degree of B-Splines, but rather to the ill-conditionedness of the matrix of the bilinear form  $a(.,.)$ . This ill-conditionedness becomes worse with the refinement of the mesh and the increase of the degree of B-Splines. A way to verify this hypothesis is to solve the linear system with a different solver, with a preconditioner applyied to the matrix before the resolution.

These simulations have been made with  $\lambda = 1.25$  and  $\mu = 1$ . We can now look at them for more realistic values of  $\lambda$  and  $\mu$ . The following table 2.1 gives the Lamé coefficients for different materials.

Material	$\lambda$ (GPa)	$\mu$ (GPa)
Steel	120	80
Concrete	17	14
Rubber	0.16	0.00033

Table 2.1: Lamé coefficients for different materials

As we can see in figure 2.8, in the case of concrete and steel, the errors behaves as expected

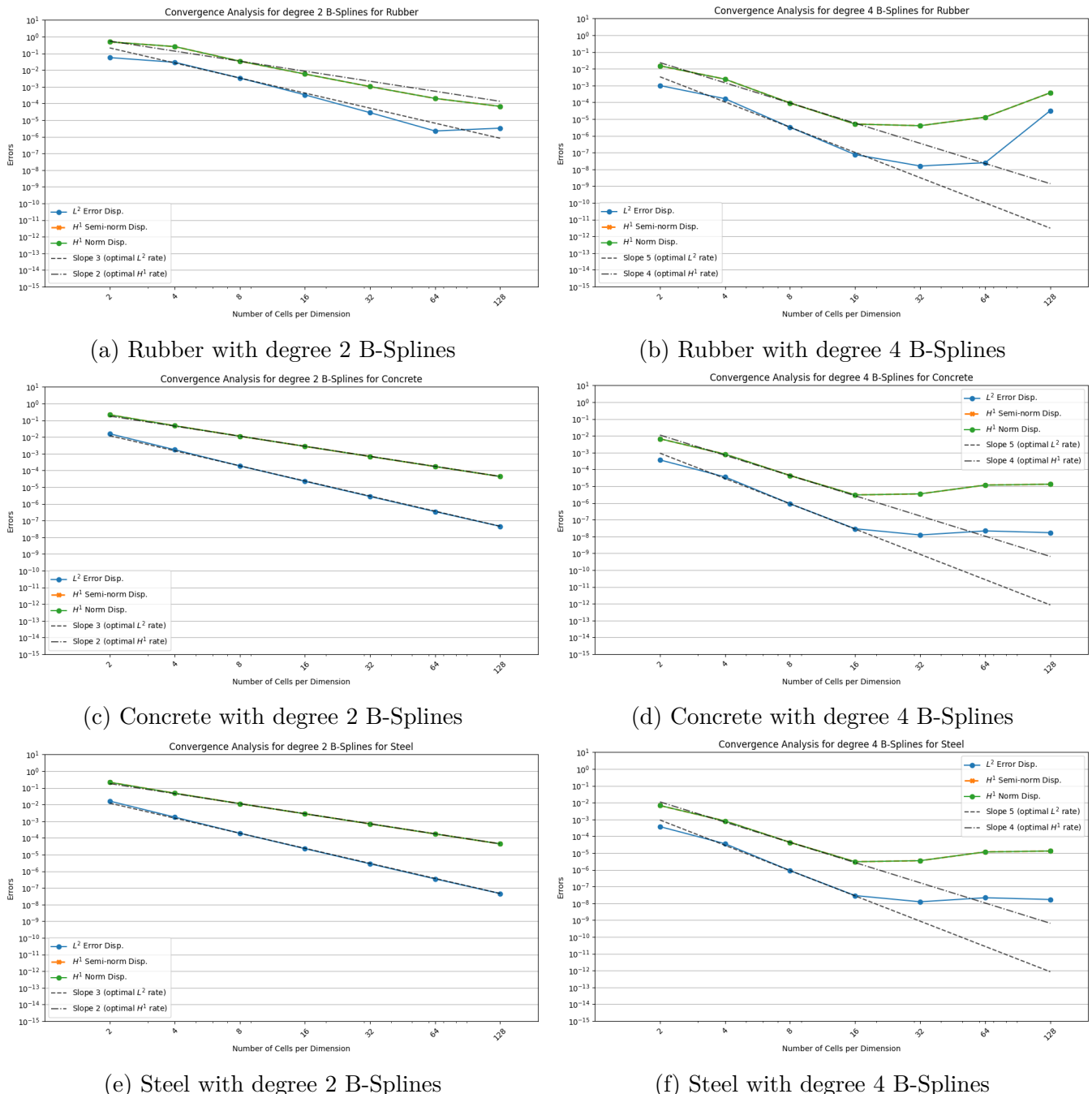


Figure 2.8: Error plots between exact solution and numerical solution with realistic values of Lam  s coefficients with degree 2 and 4 B-Splines

: well convergence with expected order and the plateau effect appears after a certain value of the error. But for the rubber, the convergence order is not really respected, the error decreases faster than expected and the plateau degenerates... To explain this, we can look at the estimates (2.6) :  $\|\vec{u} - \vec{u}^h\|_{H^1(\Omega)} \lesssim \frac{3\lambda+2\mu}{2\mu C} h^d \|\vec{u}\|_{H^{d+1}(\Omega)}$ . As  $\lambda$  is very high compared to  $\mu$ , the estimates are not really valid anymore, as  $\frac{3\lambda+2\mu}{2\mu C} \rightarrow +\infty$  when  $\lambda \rightarrow +\infty$ . This is the case for incompressible materials, like rubber, where  $\lambda$  is very high compared to  $\mu$ . To get a better idea of the convergence, we can look at the error plots for different values of  $\lambda$  with  $\mu = 1$ .

As we can see in figure 2.9, the convergence order is not respected anymore when  $\lambda$  is too high compared to  $\mu$ . We can observe that when  $\frac{\lambda}{\mu} = 10^4$ , the error behaves like the error curves for

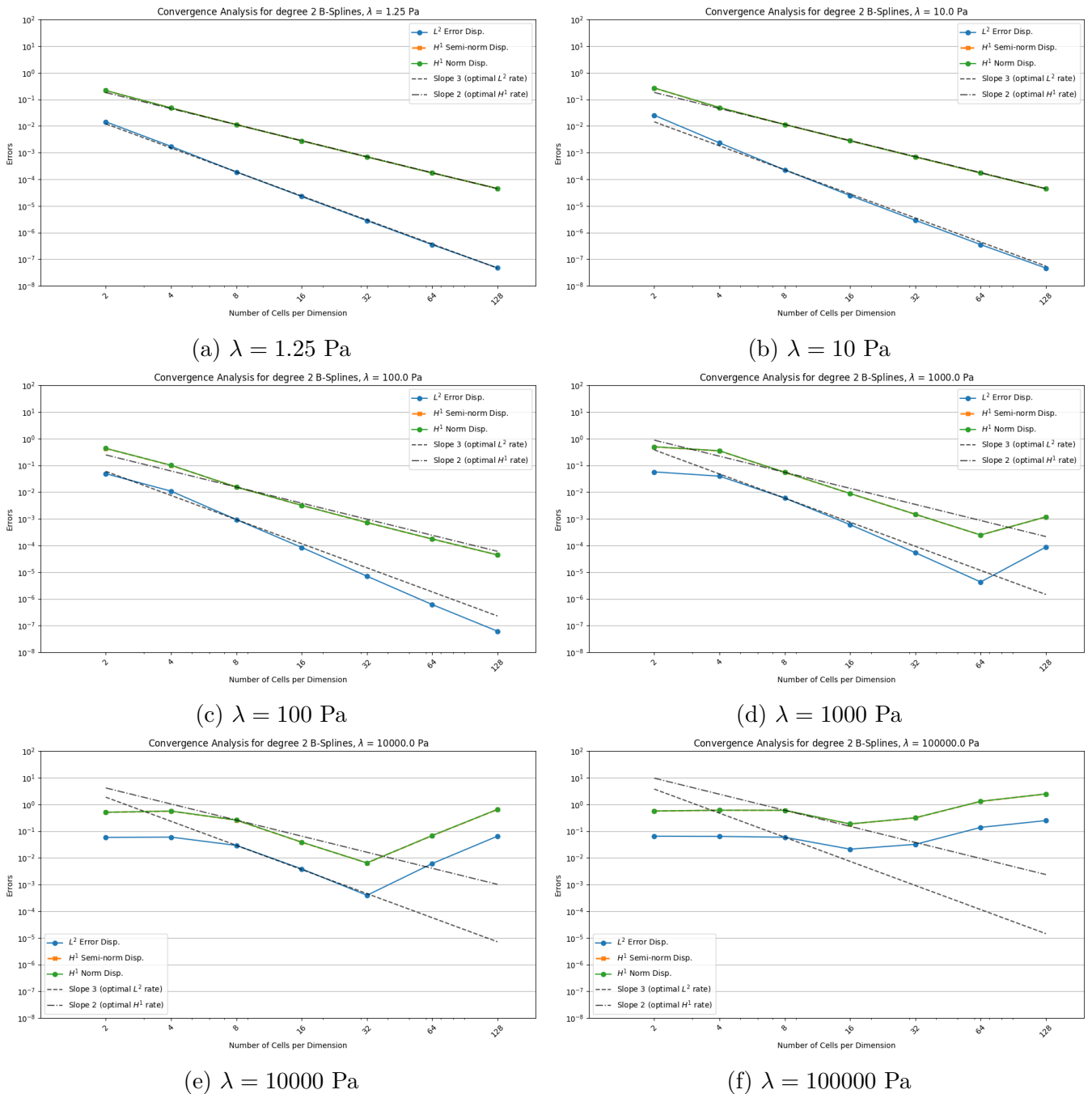


Figure 2.9: Error plots between exact solution and numerical solution with degree 2 B-Splines with increasing values of  $\lambda$  with  $\mu = 1 \text{ Pa}$

the rubber with degree 2 B-Splines in figure 2.8a  $\left(\frac{\lambda_{\text{rubber}}}{\mu_{\text{rubber}}} \approx 500\right)$ . Then, for values of  $\lambda$  such that  $\frac{\lambda}{\mu} \geq 10^4$ , the error is not even decreasing anymore.

Two hypothesis can be made to explain this phenomena :

- The estimates (2.6) are not valid anymore, as  $\lambda$  is too high compared to  $\mu$ .
- The bilinear form  $a(., .)$  is ill-conditioned, leading to numerical instability when  $\lambda$  is "too high" compared to  $\mu$ .

One can try to increase the degree of B-Splines to see if the convergence is reinforced as the power of  $h$  in the estimates is higher.

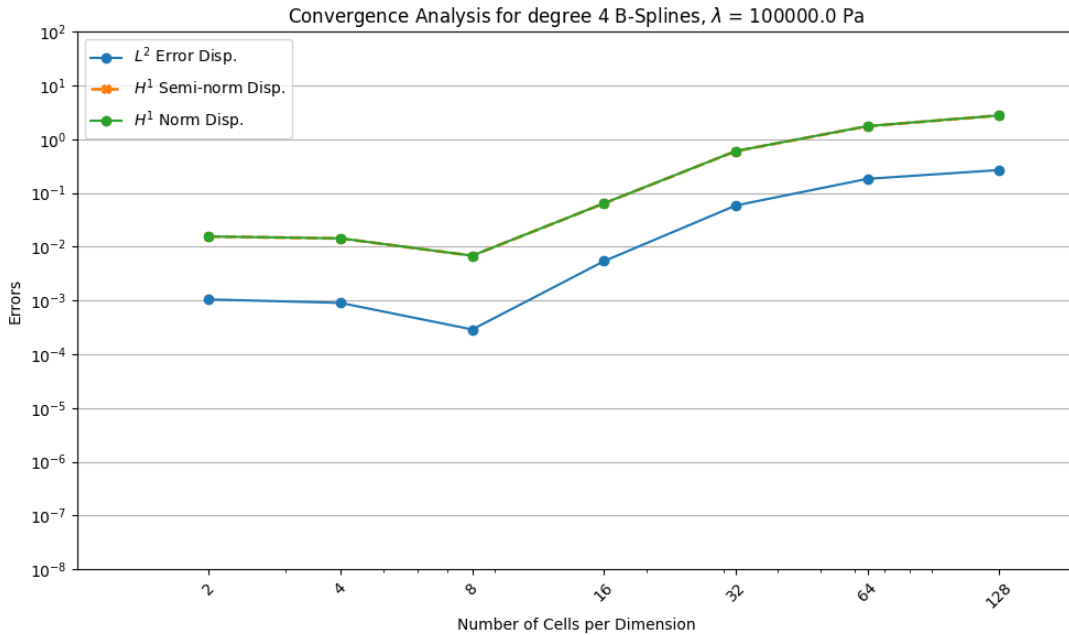


Figure 2.10: Error plot between exact solution and numerical solution with degree 4 B-Splines with  $\lambda = 100000$  Pa and  $\mu = 1$  Pa

As we can see in figure 2.10, the convergence is not reinforced, the error is still not decreasing. Actually, this phenomena is called **locking** and it is a well-known issue in FEM for incompressible materials. The locking occurs when the numerical solution is too stiff and does not converge to the real solution for high values of  $\lambda$  compared to  $\mu$ . One way to avoid this issue is to use a mixed formulation, where the pressure field is introduced as an additional variable. This will be presented in the next section.

## 2.4 Mixed displacement-pressure formulation

To introduce this formulation, let's consider again the strong formulation from (2.3). Then, denotes by  $p$  the pressure field, defined by  $p = -\lambda \nabla \cdot \vec{u}$ . As we are seeking  $\vec{u} \in \mathbf{H}^1(\Omega)$ ,  $p$  is naturally living in  $L^2(\Omega)$ . Then Hook's law can be rewritten :  $\sigma(\vec{u}, p) = -pI_3 + 2\mu\varepsilon(\vec{u})$  in  $\Omega$

So the strong formulation can be re-write as : For a given  $\vec{f} \in \mathbf{L}^2(\Omega)$ ,  $\vec{t}_N \in \mathbf{L}^2(\partial\Omega_N)$ , find  $(\vec{u}, p) \in \mathbf{H}^1(\Omega) \times L^2(\Omega)$  such that :

$$\begin{cases} -\nabla \cdot \sigma(\vec{u}, p) = \vec{f} & \text{in } \Omega \quad (\text{Equilibrium}) \\ \nabla \cdot \vec{u} + \frac{1}{\lambda}p = 0 & \text{in } \Omega \quad (\text{Pressure field definition}) \\ \vec{u} = \vec{0} & \text{in } \partial\Omega_D \\ \sigma(\vec{u}) \cdot \vec{n} = \vec{t}_N & \text{in } \partial\Omega_N \end{cases} \quad (2.7)$$

Now, to derive the weak formulation associated, first we multiply the Equilibrium equation by  $v \in \mathbf{H}_{0,D}^1(\Omega)$  and we interger by part on  $\Omega$ , then we multiply the Pressure field equation by  $q \in L^2(\Omega)$  and we interger over  $\Omega$ . Then we just have to add both integrals. Then, the weak formulation is:

$$\begin{cases} \text{Find } (\vec{u}, p) \in \mathbf{H}_{0,D}^1(\Omega) \times L^2(\Omega) \text{ such that :} \\ \tilde{a}((\vec{u}, p), (\vec{v}, q)) = l(\vec{v}, q) \quad \forall (\vec{v}, q) \in \mathbf{H}_{0,D}^1(\Omega) \times L^2(\Omega) \end{cases} \quad (2.8)$$

With :

$$\begin{aligned}\tilde{a} : & \left\{ \begin{array}{l} (\mathbf{H}_{\bar{0},D}^1(\Omega) \times L^2(\Omega))^2 \rightarrow \mathbb{R} \\ ((\vec{u}, p), (\vec{v}, q)) \mapsto \int_{\Omega} \left( 2\mu \boldsymbol{\varepsilon}(\vec{u}) : \boldsymbol{\varepsilon}(\vec{v}) - p(\boldsymbol{\nabla} \cdot \vec{v}) + (\boldsymbol{\nabla} \cdot \vec{u})q + \frac{1}{\lambda}pq \right) dV \end{array} \right. \\ l : & \left\{ \begin{array}{l} \mathbf{H}_{\bar{0},D}^1(\Omega) \rightarrow \mathbb{R} \\ \vec{v} \mapsto \int_{\Omega} \vec{f} \cdot \vec{v} dV + \int_{\partial\Omega_N} \vec{t}_N \cdot \vec{v} dS \end{array} \right.\end{aligned}$$

### 2.4.1 Well-posedness of the mixed displacement–pressure formulation

Let

$$V := \mathbf{H}_{\bar{0},D}^1(\Omega), \quad Q := L^2(\Omega), \quad X := V \times Q,$$

with the product norm

$$\|(\vec{u}, p)\|_X^2 := \|\vec{u}\|_{\mathbf{H}^1(\Omega)}^2 + \|p\|_{L^2(\Omega)}^2.$$

Now, we can prove the well-posedness of (2.8) for every finite  $\lambda > 0, \mu > 0$  and  $\Omega_D \neq \emptyset$ .

- $(X, \|\cdot\|_X)$  is a Hilbert space.
- $\tilde{a}(\cdot, \cdot)$  is a bilinear form on  $X \times X$  and  $l(\cdot)$  is linear on  $X$ .
- $l(\cdot)$  is continuous: for all  $(\vec{v}, q) \in X$ ,

$$\begin{aligned}|l(\vec{v}, q)| &\leq |(\vec{f}, \vec{v})_{L^2(\Omega)}| + |(\vec{t}_N, \vec{v})_{L^2(\partial\Omega_N)}| \\ &\leq \left( \|\vec{f}\|_{L^2(\Omega)} + C_{\text{tr}} \|\vec{t}_N\|_{L^2(\partial\Omega_N)} \right) \|\vec{v}\|_{H^1(\Omega)} \\ |l(\vec{v}, q)| &\leq C \left( \|\vec{f}\|_{L^2(\Omega)} + \|\vec{t}_N\|_{L^2(\partial\Omega_N)} \right) \|(\vec{v}, q)\|_X,\end{aligned}$$

where  $C_{\text{tr}}$  is the trace constant and  $C$  a generic constant.

- $\tilde{a}(\cdot, \cdot)$  is continuous: for all  $(\vec{u}, p), (\vec{v}, q) \in X$ ,

$$\begin{aligned}|\tilde{a}((\vec{u}, p), (\vec{v}, q))| &\leq 2\mu \|\boldsymbol{\varepsilon}(\vec{u})\|_{L^2} \|\boldsymbol{\varepsilon}(\vec{v})\|_{L^2} + \|p\|_{L^2} \|\boldsymbol{\nabla} \cdot \vec{v}\|_{L^2} + \|\boldsymbol{\nabla} \cdot \vec{u}\|_{L^2} \|q\|_{L^2} + \frac{1}{\lambda} \|p\|_{L^2} \|q\|_{L^2} \\ &\leq 2\mu \|\vec{u}\|_{\mathbf{H}^1} \|\vec{v}\|_{\mathbf{H}^1} + 3\|p\|_{L^2} \|\vec{v}\|_{\mathbf{H}^1} + 3\|\vec{u}\|_{\mathbf{H}^1} \|q\|_{L^2} + \frac{1}{\lambda} \|p\|_{L^2} \|q\|_{L^2} \\ &\leq 2\mu \|(\vec{u}, p)\|_X \|(\vec{v}, q)\|_X + 3\|(\vec{u}, p)\|_X \|(\vec{v}, q)\|_X + 3\|(\vec{u}, p)\|_X \|(\vec{v}, q)\|_X \\ &\quad + \frac{1}{\lambda} \|(\vec{u}, p)\|_X \|(\vec{v}, q)\|_X \\ |\tilde{a}((\vec{u}, p), (\vec{v}, q))| &\leq (2\mu + 6 + \frac{1}{\lambda}) \|(\vec{u}, p)\|_X \|(\vec{v}, q)\|_X.\end{aligned}$$

using  $\|\boldsymbol{\nabla} \cdot \vec{w}\|_{L^2} \leq 3\|\vec{w}\|_{H^1}$ ,  $\|p\|_{L^2} \leq \|(\vec{u}, p)\|_X$  and  $\|\vec{u}\|_{H^1} \leq \|(\vec{u}, p)\|_X$ .

- $\tilde{a}(\cdot, \cdot)$  is coercive on  $X$ : for all  $(\vec{u}, p) \in X$ ,

$$\tilde{a}((\vec{u}, p), (\vec{u}, p)) = 2\mu \|\boldsymbol{\varepsilon}(\vec{u})\|_{L^2}^2 + \frac{1}{\lambda} \|p\|_{L^2}^2 \geq 2\mu C_K^2 \|\vec{u}\|_{H^1}^2 + \frac{1}{\lambda} \|p\|_{L^2}^2 \geq \alpha \|(\vec{u}, p)\|_X^2,$$

with  $\alpha := \min\{2\mu C_K^2, 1/\lambda\} > 0$  (for fixed finite  $\lambda$ ).

Then, by Lax–Milgram theorem, the mixed problem (2.8) admits a unique solution  $(\vec{u}, p) \in X$  and the stability estimate

$$\|\vec{u}\|_{H^1(\Omega)} + \|p\|_{L^2(\Omega)} \leq C \left( \|\vec{f}\|_{L^2(\Omega)} + \|\vec{t}_N\|_{L^2(\partial\Omega_N)} \right)$$

holds with  $C$  independent of  $(\vec{f}, \vec{t}_N)$ .

**Remark.** As  $\lambda \rightarrow \infty$  (near-incompressible limit) the coercivity constant degenerates on the pressure component; the formulation approaches a saddle-point (Stokes-like) problem requiring an inf-sup (Ladyzhenskaya–Babuška–Brezzi) condition on the pair  $(V, Q)$  to remain stable.

A way to ensure the inf-sup condition is to impose a non-zero mean value for the pressure field, i.e.,  $p \in L_0^2(\Omega)$ , which is a common practice in numerical simulations of incompressible flows.

Then, the following inf-sup condition holds:

$$\inf_{q \in Q} \sup_{\vec{v} \in V} \frac{\tilde{a}((\vec{v}, q), (\vec{u}, p))}{\|\vec{v}\|_{H^1(\Omega)} \|q\|_{L^2(\Omega)}} \geq \beta > 0,$$

for some  $\beta > 0$  independent of  $\lambda$  and  $\mu$ . This condition ensures the stability of the mixed formulation and prevents spurious oscillations in the pressure field, and  $V = H_0^1(\Omega)$  and  $Q = L_0^2(\Omega)$  [Bof+08].

If  $\Omega_D = \emptyset$ , the Dirichlet boundary condition is not imposed, and the problem becomes a pure Stokes problem. In this case, the inf-sup condition is necessary to ensure the well-posedness of the problem, and the uniqueness of the solution is guaranteed by the compatibility condition on the external loads, as discussed in Section ?? modulo a rigid body motion.

#### 2.4.2 Isogeometric discretisation and a priori error estimate

Under standard approximation and stability assumptions for the mixed formulation, the Galerkin solution enjoys the usual quasi-optimal a priori estimate. Let  $(V_h, Q_h) \subset V \times Q$  be the tensor–product B-spline spaces of (vector) degree  $d$  (for the displacement) and (scalar) degree  $d$  or  $d - 1$  (for the pressure) with mesh size  $h$ , and assume that the discrete inf–sup condition holds with a constant  $\beta > 0$  independent of  $h$ ,  $\lambda$  and  $\mu$  (locking-free setting) [Bof+08]. Then, for the exact solution  $(\vec{u}, p)$  of (2.8) and the discrete solution  $(\vec{u}_h, p_h) \in V_h \times Q_h$ , continuity plus coercivity on the kernel give the Céa type bound

$$\|\vec{u} - \vec{u}_h\|_{H^1(\Omega)} + \|p - p_h\|_{L^2(\Omega)} \leq C \left( \inf_{\vec{w}_h \in V_h} \|\vec{u} - \vec{w}_h\|_{H^1(\Omega)} + \inf_{q_h \in Q_h} \|p - q_h\|_{L^2(\Omega)} \right),$$

with  $C$  independent of  $h, \lambda, \mu$ . For  $(\vec{u}, p)$  sufficiently smooth, namely  $\vec{u} \in \mathbf{H}^{d+1}(\Omega)$  and  $p \in H^d(\Omega)$ , spline approximation estimates yield

$$\|\vec{u} - \vec{u}_h\|_{H^1(\Omega)} + \|p - p_h\|_{L^2(\Omega)} \leq Ch^d \left( \|\vec{u}\|_{\mathbf{H}^{d+1}(\Omega)} + \|p\|_{H^d(\Omega)} \right),$$

and, under the additional elliptic regularity needed for a duality argument, the displacement  $L^2$ -error improves to

$$\|\vec{u} - \vec{u}_h\|_{L^2(\Omega)} \leq Ch^{d+1} \|\vec{u}\|_{\mathbf{H}^{d+1}(\Omega)}.$$

Crucially, these constants remain bounded as  $\lambda \rightarrow \infty$ , in contrast with the pure displacement formulation whose coercivity deteriorates ( $\alpha \sim 1/\lambda$ ), leading to volumetric locking; hence the mixed formulation delivers uniform (locking-free) convergence in the nearly incompressible regime [Bof+08; DV+14].

### 2.4.3 Example of simulation using PSYDAC

In this section, we will present the results of a simulation using the mixed displacement-pressure formulation with B-Splines.

For the manufactured solution, we will use the same one as in section 2.3.1. For reminder, the exact solution is given by:

$$\vec{u}_e(x, y, z) = \begin{pmatrix} 0 \\ 0 \\ \sin(\pi x) \sin(\pi y) \sin(\pi z) \end{pmatrix}, \quad p_e(x, y, z) = -\lambda \nabla \cdot \vec{u}_e = -\lambda \pi \sin(\pi x) \sin(\pi y) \cos(\pi z).$$

$$\vec{f} = -\nabla \cdot \boldsymbol{\sigma}(\vec{u}_e, p_e) = \begin{pmatrix} -\pi^2(\lambda + \mu) \cos(\pi x) \sin(\pi y) \cos(\pi z) \\ -\pi^2(\lambda + \mu) \sin(\pi x) \cos(\pi y) \cos(\pi z) \\ \pi^2(\lambda + 4\mu) \sin(\pi x) \sin(\pi y) \sin(\pi z) \end{pmatrix}.$$

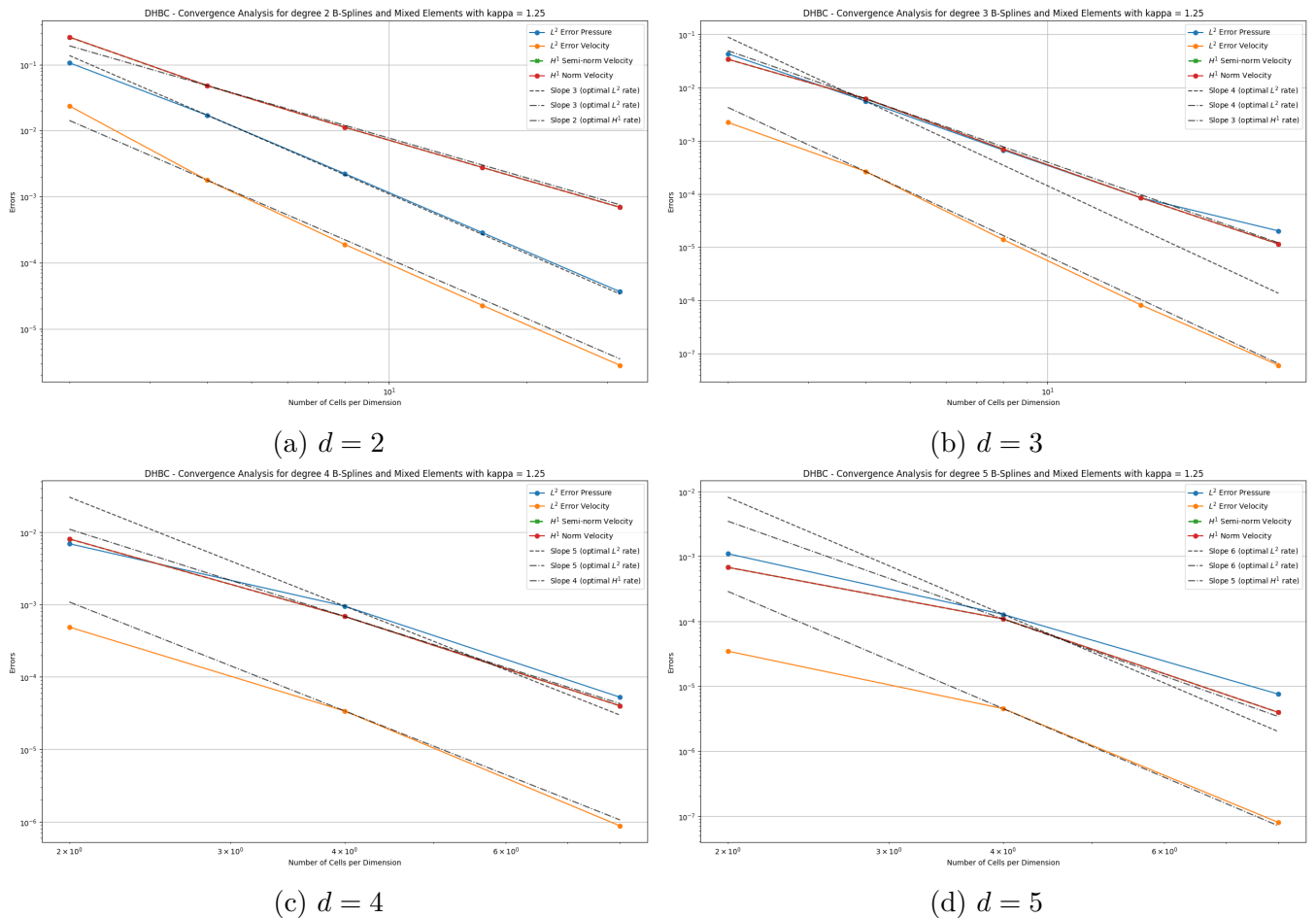


Figure 2.11: Four plots of errors between exact solution and numerical solution with different degree B-Splines (with  $\lambda = 1.25$  and  $\mu = 1$ ) using the mixed formulation

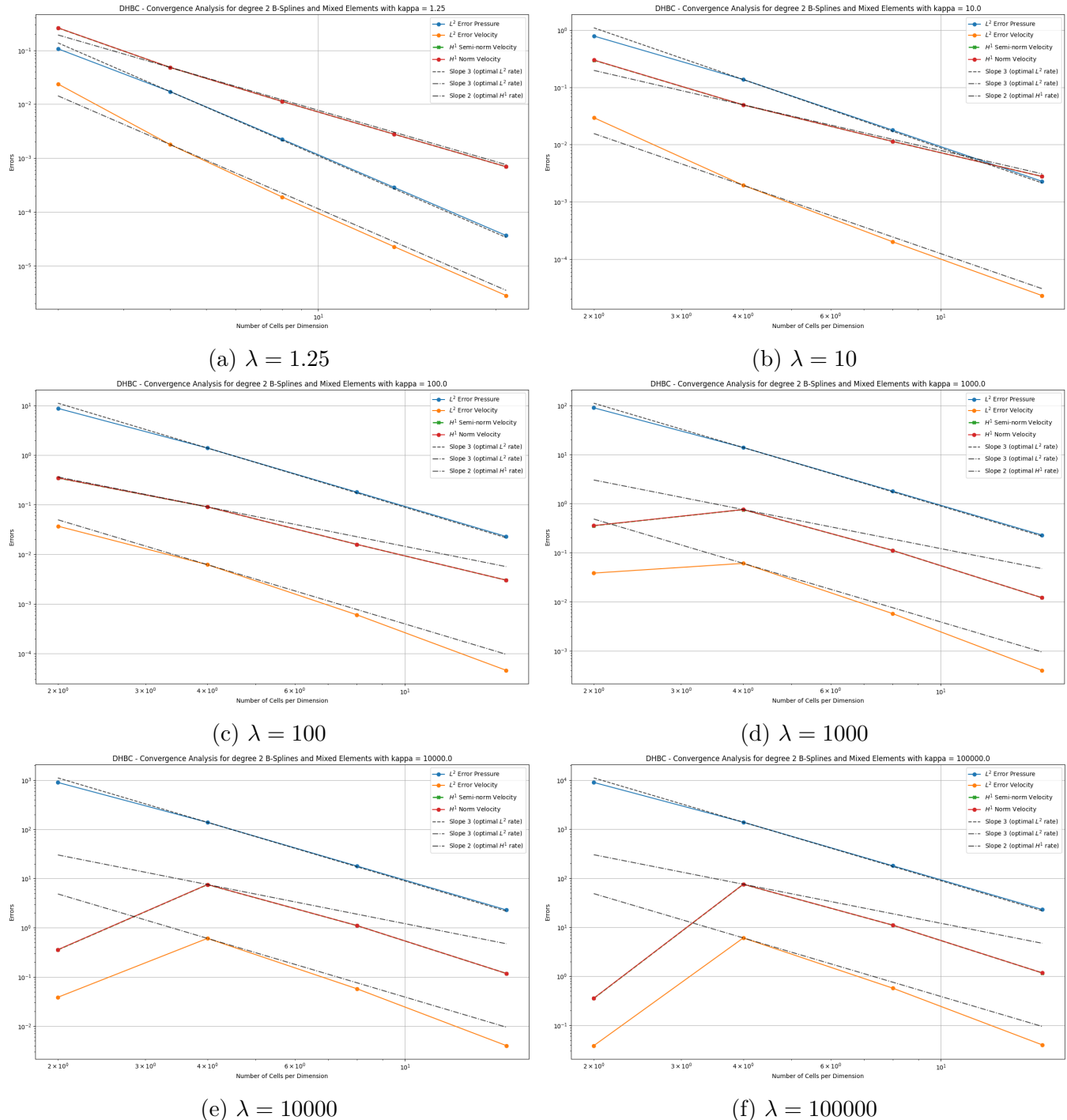


Figure 2.12: Error plots between exact solution and numerical solution with degree 2 B-Splines and mixed formulation with increasing values of  $\lambda$

# Chapter 3

## Thermoelasticity

### 3.1 Introduction

This chapter is dedicated to the study of the thermoelasticity problem, which is a coupled problem between the mechanical and thermal fields. The aim is to solve the coupled system of equations that govern the behavior of a thermoelastic material under thermal and mechanical loads. This work has been initiated to solve a problem present during the IPP Programme Days 2025 by Prof. Dr. Rudolf Neu. The goal is to understand the deformation of a medium under the influence of thermal loads and mechanical forces. The medium is composite material, composed of copper and tungsten. The geometry is presented on the following figure.

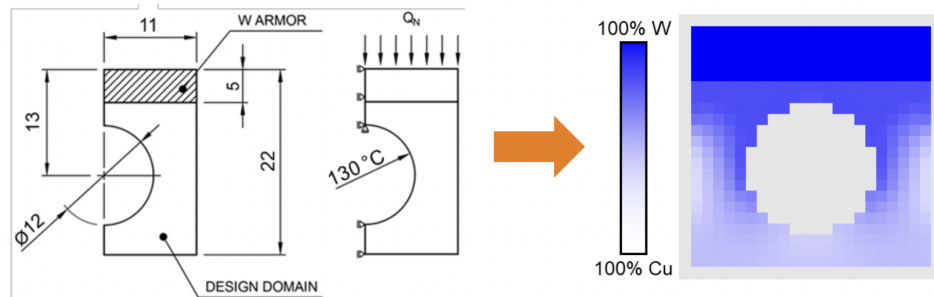


Figure 3.1: Geometry of the thermoelasticity problem from the IPP Programme Days 2025

### 3.2 Simplified problem - Physical model and equations

Before solving this problem, I want to simplify it a bit by considering a slightly different geometry, which is a square without the hole in the middle. The goal is to understand the behavior of the medium under thermal and mechanical loads, to see how the deformation of the medium is affected by the thermal loads and to see if PSYDAC can effectively solve this simplified problem. The geometry of the simplified problem is presented on the figure 3.2.

#### 3.2.1 Problem setup and parameters

The problem can be parameterized as follows with other boundary conditions and parameters:

- The domain  $\Omega$  is a square of size 22:  $\Omega = [0, 22]^2$ .

- $\partial\Omega_{\text{heat}} = \{(x, y) \in \partial\Omega \mid x = 0 \text{ and } x = 22\}$  is the left and right edges of the square, where heat  $Q$  is applied.  $\partial\Omega_{\text{temp}} = \{(x, y) \in \partial\Omega \mid y = 0 \text{ and } y = 22\}$  is the top and bottom edges of the square, where the temperature is fixed to  $T_0$ .
- $\partial\Omega_D = \{(x, y) \in \partial\Omega \mid x = 0 \text{ and } x = 22\}$  is the left and right edges of the square, where the Dirichlet boundary conditions are applied and the displacement is fixed.  $\partial\Omega_N = \{(x, y) \in \partial\Omega \mid y = 0 \text{ and } y = 22\}$  is the top and bottom edges of the square, where the Neumann boundary conditions are applied and the traction is fixed.
- For  $y \in (0, 17)$ , the material is composite and properties are given by a affine interpolation between the properties of copper and tungsten. For  $y \in (17, 22)$ , the material is pure tungsten. For example,  $\lambda$  is defined as:

$$\lambda(y) = \begin{cases} \lambda_{\text{Cu}} + \frac{y}{17}(\lambda_{\text{W}} - \lambda_{\text{Cu}}) & \text{if } y \in (0, 17) \\ \lambda_{\text{W}} & \text{if } y \in (17, 22) \end{cases}$$

- The material properties are given by:

Property	Cu	W
Lamé's first constant $\lambda$ [Pa]	$1.1 \times 10^{11}$	$2.5 \times 10^{11}$
Shear modulus $\mu$ [Pa]	$4.1 \times 10^{10}$	$1.6 \times 10^{11}$
Thermal expansion $\alpha$ [1/K]	$1.7 \times 10^{-5}$	$4.5 \times 10^{-6}$
Thermal conductivity $\kappa$ [W/(m·K)]	401	174

Table 3.1: Material properties of Copper (Cu) and Tungsten (W).

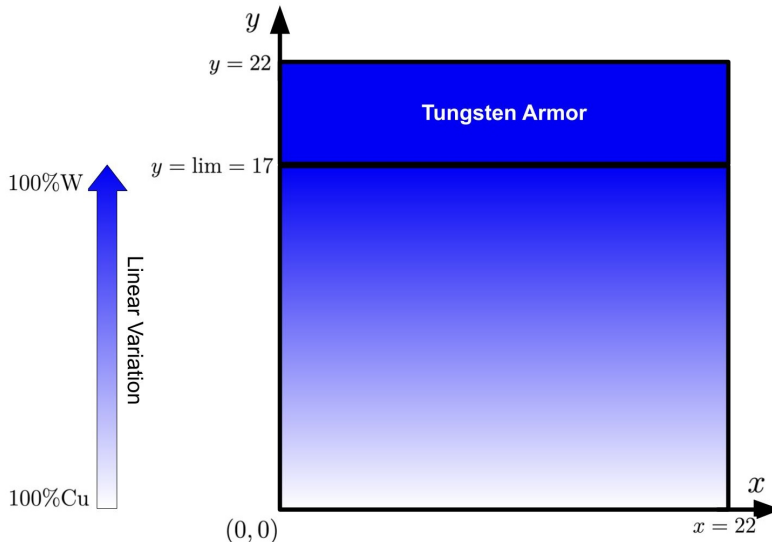


Figure 3.2: Geometry of the simplified thermoelasticity problem

### 3.2.2 Strong Formulation

The presentation of the strong formulation of the thermoelasticity problem is based on the principles of continuum mechanics and thermodynamics taken from [MS15] and [Per16]. The thermoelasticity problem is a coupled problem between the mechanical and thermal fields. The equations

that govern the behavior of a thermoelastic material are given by the coupling of the heat equation and the elasticity equation.

The full time-dependent thermoelasticity equations are:

$$\begin{cases} \rho(y)c_p(y)\frac{\partial T}{\partial t} + \nabla \cdot (\kappa(y)\nabla T) = Q - (3\lambda(y) + 2\mu(y))\alpha(y)T_0\frac{\partial}{\partial t}(\nabla \cdot \vec{u}) \\ \rho(y)\frac{\partial^2 \vec{u}}{\partial t^2} - \nabla \cdot \boldsymbol{\sigma}(\vec{u}) = \vec{f} \\ \boldsymbol{\sigma}(\vec{u}) = \lambda(y)(\nabla \cdot \vec{u})I_3 + 2\mu(y)\boldsymbol{\varepsilon}(\vec{u}) - (3\lambda(y) + 2\mu(y))\alpha(y)TI_3 \end{cases} \quad (3.1)$$

where  $\rho(y)$  is the density,  $c_p(y)$  is the specific heat capacity at constant pressure,  $T$  is the temperature,  $\kappa(y)$  is the thermal conductivity,  $Q$  is the heat source,  $\vec{u}$  is the displacement field,  $\vec{f}$  is the body force,  $\boldsymbol{\sigma}$  is the stress tensor,  $\lambda(y)$  and  $\mu(y)$  are the Lamé coefficients,  $\boldsymbol{\varepsilon}$  is the strain tensor,  $\alpha(y)$  is the thermal expansion coefficient and  $T_0$  is the reference temperature.

For this study, we will consider the stationary case, where the time derivatives are zero ( $\frac{\partial T}{\partial t} = 0$  and  $\frac{\partial^2 \vec{u}}{\partial t^2} = 0$ ). This simplifies the system to:

$$\begin{cases} -\nabla \cdot (\kappa(y)\nabla T) = Q \\ -\nabla \cdot \boldsymbol{\sigma}(\vec{u}) = \vec{f} \\ \boldsymbol{\sigma}(\vec{u}) = \lambda(y)(\nabla \cdot \vec{u})I_3 + 2\mu(y)\boldsymbol{\varepsilon}(\vec{u}) - (3\lambda(y) + 2\mu(y))\alpha(y)TI_3 \end{cases}$$

These stationary equations represent the equilibrium state of the thermoelastic material under constant thermal and mechanical loads.

To complete the problem formulation, we must specify the boundary conditions. Based on the problem description, we have the following conditions on the boundary  $\partial\Omega$ :

For the thermal problem:

$$T = T_0 \quad \text{on } \partial\Omega_{\text{temp}} \quad (3.2)$$

$$-\kappa\nabla T \cdot \vec{n} = q_S \quad \text{on } \partial\Omega_{\text{heat}} \quad (3.3)$$

where  $T_0$  is the reference temperature and  $q_S$  is the applied heat flux on the boundary.

For the mechanical problem:

$$\vec{u} = \vec{u}_D \quad \text{on } \partial\Omega_D \quad (3.4)$$

$$\boldsymbol{\sigma}(\vec{u}) \cdot \vec{n} = \vec{t}_N \quad \text{on } \partial\Omega_N \quad (3.5)$$

where  $\vec{u}_D$  is the prescribed displacement and  $\vec{t}_N$  is the prescribed traction. To prove the well-posedness of the problem, we will limit the analysis to  $T_0 = 0$  and  $\vec{u}_D = \vec{0}$ , otherwise the problem can be rewritten with homogeneous boundary conditions with a change of variables.

For a given  $Q \in L^2(\Omega)$ ,  $q_S \in L^2(\partial\Omega_{\text{heat}})$ ,  $\vec{f} \in \mathbf{L}^2(\Omega)$ ,  $\vec{t}_N \in \mathbf{L}^2(\partial\Omega_N)$ , the entire strong problem is:

Find  $(T, \vec{u}) \in H^1(\Omega) \times \mathbf{H}_{\vec{0}, D}^1(\Omega)$  such that:

$$-\nabla \cdot (\kappa(y)\nabla T) = Q \quad \text{on } \Omega \quad (3.6)$$

$$-\nabla \cdot \boldsymbol{\sigma}(\vec{u}) = \vec{f} \quad \text{on } \Omega \quad (3.7)$$

$$\boldsymbol{\sigma}(\vec{u}) = \lambda(y)(\nabla \cdot \vec{u})I_3 + 2\mu(y)\boldsymbol{\varepsilon}(\vec{u}) - (3\lambda(y) + 2\mu(y))\alpha(y)TI_3 \quad \text{on } \Omega \quad (3.8)$$

$$\vec{u} = \vec{0} \quad \text{on } \partial\Omega_D \quad (3.9)$$

$$\boldsymbol{\sigma}(\vec{u}) \cdot \vec{n} = \vec{t}_N \quad \text{on } \partial\Omega_N \quad (3.10)$$

$$T = 0 \quad \text{on } \partial\Omega_{\text{temp}} \quad (3.11)$$

$$-\kappa(y)\nabla T \cdot \vec{n} = q_S \quad \text{on } \partial\Omega_{\text{heat}} \quad (3.12)$$

This problem can be seen as a coupled thermo-mechanical problem, where the temperature field  $T$  affects the mechanical behavior of the material through the thermal expansion term in the stress tensor  $\boldsymbol{\sigma}(\vec{u})$ , but the mechanical displacement  $\vec{u}$  does not directly affect the temperature field  $T$ . So, to solve this problem, one can first solve the thermal problem to obtain the temperature field  $T$ , and then use this temperature field to solve the mechanical problem for the displacement  $\vec{u}$  with a modified source term that includes the thermal expansion effects. As  $\forall y \in [0, 22]$ ,  $\frac{\lambda(y)}{\mu(y)} \leq 50$ , according to results from Subsection 2.3.2, we can use the pure displacement formulation to solve the mechanical problem.

### 3.2.3 Weak Formulation

The corresponding weak formulation is obtained by multiplying the PDEs by suitable test functions, integrating over the domain  $\Omega$ , and applying integration by parts.

Let the solution space for temperature be  $H_{0,\text{temp}}^1 = \{\phi \in H^1(\Omega) \mid \phi = 0 \text{ on } \partial\Omega_{\text{temp}}\}$  and for displacement be  $\mathbf{H}_{0,D}^1(\Omega)$ . The weak problem is:

Find  $(T, \vec{u}) \in H_{0,\text{temp}}^1 \times \mathbf{H}_{0,D}^1(\Omega)$  such that for all test functions  $(\theta, \vec{v}) \in H_{0,\text{temp}}^1 \times \mathbf{H}_{0,D}^1(\Omega)$ :

$$\begin{cases} b(T, \theta) = l_T(\theta) \\ a(\vec{u}, \vec{v}) = l_U(\vec{v}) \end{cases} \quad (3.13)$$

With

$$\begin{aligned} b : & \left\{ \begin{array}{l} H_{0,\text{temp}}^1 \times H_{0,\text{temp}}^1 \rightarrow \mathbb{R} \\ (T, \theta) \mapsto \int_{\Omega} \kappa(y) \nabla T \cdot \nabla \theta \, d\Omega \end{array} \right. \\ l_T : & \left\{ \begin{array}{l} H_{0,\text{temp}}^1 \rightarrow \mathbb{R} \\ \int_{\Omega} Q\theta \, d\Omega - \int_{\partial\Omega_{\text{heat}}} q_S \theta \, dS \end{array} \right. \\ a : & \left\{ \begin{array}{l} \mathbf{H}_{0,D}^1(\Omega) \times \mathbf{H}_{0,D}^1(\Omega) \rightarrow \mathbb{R} \\ (\vec{u}, \vec{v}) \mapsto \int_{\Omega} \left( \lambda(y) (\nabla \cdot \vec{u})(\nabla \cdot \vec{v}) + 2\mu(y) \boldsymbol{\epsilon}(\vec{u}) : \boldsymbol{\epsilon}(\vec{v}) \right) \, d\Omega \end{array} \right. \\ l_U : & \left\{ \begin{array}{l} \mathbf{H}_{0,D}^1(\Omega) \rightarrow \mathbb{R} \\ \int_{\Omega} \vec{f} \cdot \vec{v} \, d\Omega + \int_{\partial\Omega_N} \vec{t}_N \cdot \vec{v} \, dS + \int_{\Omega} (3\lambda(y) + 2\mu(y)) \alpha(y) T (\nabla \cdot \vec{v}) \, d\Omega \end{array} \right. \end{aligned}$$

$\exists \kappa_-, \kappa_+, \lambda_-, \lambda_+, \mu_-, \mu_+, \alpha_-, \alpha_+ > 0$  such that  $\forall y \in [0, 22]$ ,

$0 < \kappa_- \leq \kappa(y) \leq \kappa_+ < +\infty \quad 0 < \lambda_- \leq \lambda(y) \leq \lambda_+ < +\infty$

$0 < \mu_- \leq \mu(y) \leq \mu_+ < +\infty \quad 0 < \alpha_- \leq \alpha(y) \leq \alpha_+ < +\infty$ .

Now, we prove the well-posedness of the thermal problem.

- $(H_{0,\text{heat}}^1(\Omega), \|\cdot\|_{H^1(\Omega)})$  is a Hilbert space.
- $a(\cdot, \cdot)$  is a bilinear form on  $H_{0,\text{heat}}^1(\Omega) \times H_{0,\text{heat}}^1(\Omega)$  and  $\ell_T$  is a linear form on  $H_{0,\text{heat}}^1(\Omega)$ .
- $\ell_T(\cdot)$  is continuous: by Cauchy–Schwarz and the trace inequality,

$$\begin{aligned} \forall \theta \in H_{0,\text{heat}}^1(\Omega), \quad |\ell_T(\theta)| & \leq \|Q\|_{L^2(\Omega)} \|\theta\|_{L^2(\Omega)} + \|q_S\|_{L^2(\partial\Omega_{\text{heat}})} \|\theta\|_{L^2(\partial\Omega_{\text{heat}})} \\ & \leq \left( \|Q\|_{L^2(\Omega)} + \|\gamma_0\| \|q_S\|_{L^2(\partial\Omega_{\text{heat}})} \right) \|\theta\|_{H^1(\Omega)}, \end{aligned}$$

where  $\gamma_0 : H^1(\Omega) \rightarrow L^2(\partial\Omega_{\text{heat}})$  is the trace operator.

- $a(\cdot, \cdot)$  is continuous:

$$\forall T, \theta \in H_{0,\text{heat}}^1(\Omega), \quad |a(T, \theta)| \leq \kappa_+ \|\nabla T\|_{L^2(\Omega)} \|\nabla \theta\|_{L^2(\Omega)} \\ \leq \kappa_+ \|T\|_{H^1(\Omega)} \|\theta\|_{H^1(\Omega)}.$$

- $a(\cdot, \cdot)$  is coercive:  $\forall T \in H_{0,\text{heat}}^1(\Omega)$ ,

$$a(T, T) = \int_{\Omega} \kappa(y) |\nabla T|^2 dx \geq \kappa_{\min} \|\nabla T\|_{L^2(\Omega)}^2 \geq \kappa_- \left( \frac{1}{2} \|\nabla T\|_{L^2(\Omega)}^2 + \frac{1}{2} \|\nabla T\|_{L^2(\Omega)}^2 \right).$$

Since functions in  $H_{0,\text{heat}}^1(\Omega)$  vanish on  $\partial\Omega_{\text{temp}}$  and a Poincaré inequality holds on  $H_{0,\text{heat}}^1(\Omega)$ , there exists  $C_P > 0$  such that  $\|T\|_{L^2(\Omega)} \leq C_P \|\nabla T\|_{L^2(\Omega)}$ .

$$a(T, T) \geq \kappa_- \left( \frac{1}{2} \|\nabla T\|_{L^2(\Omega)}^2 + \frac{1}{2C_P^2} \|T\|_{L^2(\Omega)}^2 \right) \geq \alpha \|T\|_{H^1(\Omega)}^2$$

With  $\alpha = \min \left( \frac{\kappa_-}{2}, \frac{\kappa_-}{2C_P^2} \right) > 0$ .

Therefore  $a(\cdot, \cdot)$  is continuous and coercive on the Hilbert space  $H_{0,\text{heat}}^1(\Omega)$ , and  $\ell_T \in H_{0,\text{heat}}^1(\Omega)'$ . By the Lax–Milgram theorem there exists a unique  $T \in H_{0,\text{heat}}^1(\Omega)$  such that

$$a(T, \theta) = \ell_T(\theta) \quad \forall \theta \in H_{0,\text{heat}}^1(\Omega).$$

The well-posedness of the displacement problem is similar to Section 2.2. Here, we can add that  $\ell_U$  is continuous,  $a$  is continuous and coercive with new constants:

- $\forall v \in \mathbf{H}_{0,D}^1(\Omega)$ ,

$$|\ell_U(v)| \leq \left( \|\vec{f}\|_{L^2(\Omega)} + \|\gamma_0\| \|\vec{t}_N\|_{L^2(\partial\Omega_N)} \right) \|\vec{v}\|_{H^1(\Omega)} + (3\lambda_+ + 2\mu_+) \alpha_+ \|T\|_{L^2(\Omega)} \|\nabla \cdot \vec{v}\|_{L^2(\Omega)} \\ \leq \left( \|\vec{f}\|_{L^2(\Omega)} + \|\gamma_0\| \|\vec{t}_N\|_{L^2(\partial\Omega_N)} \right) \|\vec{v}\|_{H^1(\Omega)} + 2(3\lambda_+ + 2\mu_+) \alpha_+ \|T\|_{L^2(\Omega)} \|\vec{v}\|_{H^1(\Omega)}. \\ |\ell_U(v)| \leq \left( \|\vec{f}\|_{L^2(\Omega)} + \|\gamma_0\| \|\vec{t}_N\|_{L^2(\partial\Omega_N)} + 2(3\lambda_+ + 2\mu_+) \alpha_+ \|T\|_{L^2(\Omega)} \right) \|\vec{v}\|_{H^1(\Omega)}.$$

- $\forall \vec{u}, \vec{v} \in \mathbf{H}_{0,D}^1(\Omega)$ ,

$$|a(\vec{u}, \vec{v})| \leq (3\lambda_+ + 2\mu_+) \|\vec{u}\|_{H^1(\Omega)} \|\vec{v}\|_{H^1(\Omega)}$$

- $\forall \vec{u} \in \mathbf{H}_{0,D}^1(\Omega)$ ,

$$|a(\vec{u}, \vec{u})| \geq 2\mu_- C \|\vec{u}\|_{H^1(\Omega)}^2$$

With  $C > 0$  a constant from Korn's inequality.

### 3.2.4 Numerical simulation

Denotes by  $V^h \subset H_{0,\text{heat}}^1(\Omega)$  a finite-dimensional subspace of test functions for temperature,  $\mathbf{V}^h \subset \mathbf{H}_{0,D}^1(\Omega)$  a finite-dimensional subspace of test functions for displacement.  $d$  is the degree of the B-spline spaces used to approximate the solution. Let's suppose that  $(T, \vec{u}) \in H^{s+1}(\Omega) \times \mathbf{H}^{s+1}(\Omega)$

for some  $s \in [1, d + 1]$  is solving (3.2.3) and let's denote the corresponding approximations by  $(T^h, \vec{u}^h) \in V^h \times \mathbf{V}^h$ . The best approximation estimates for the B-spline spaces  $V^h$  and  $\mathbf{V}^h$  is:

$$\begin{aligned} \|T - T^h\|_{H^1(\Omega)} &\leq C_1 h^q \|T\|_{H^{q+1}(\Omega)}, \\ \|T - T^h\|_{L^2(\Omega)} &\leq C_2 h^{q+1} \|T\|_{H^{q+1}(\Omega)}, \\ \|\vec{u} - \vec{u}^h\|_{\mathbf{H}^1(\Omega)} &\leq C_3 h^q \|\vec{u}\|_{\mathbf{H}^{q+1}(\Omega)}, \\ \|\vec{u} - \vec{u}^h\|_{L^2(\Omega)} &\leq C_4 h^{q+1} \|\vec{u}\|_{\mathbf{H}^{q+1}(\Omega)}. \end{aligned} \quad (3.14)$$

where  $C_1, C_2, C_3, C_4 > 0$  are constants independent of  $h$ , and  $q = \min(d, s)$  [DV+14]. To evaluate the accuracy of the numerical solution, we can use these estimates to bound the error between the exact solution and the numerical approximation and compare it with the numerical results obtained from the simulation. Again, we use the manufactured solutions approach to evaluate the performance of the numerical method.

For that purpose, we can consider  $T_e$  and  $\vec{u}_e$  defined as:

$$T_e = \cos\left(\frac{\pi x}{22}\right) \cos\left(\frac{\pi y}{22}\right) \quad \vec{u}_e = \begin{pmatrix} 0 \\ \cos\left(\frac{\pi x}{22}\right) \cos\left(\frac{\pi y}{22}\right) \end{pmatrix}$$

and the corresponding source terms:

$$\begin{aligned} Q &= -\nabla \cdot (\kappa(y) \nabla T_e), & q_S &= -\kappa(y) \nabla T_e \cdot \vec{n}, \\ \vec{f} &= -\nabla \cdot \boldsymbol{\sigma}(\vec{u}_e), & \vec{t}_N &= \boldsymbol{\sigma}(\vec{u}_e) \cdot \vec{n}. \end{aligned}$$

The first result I obtained was the following plot:

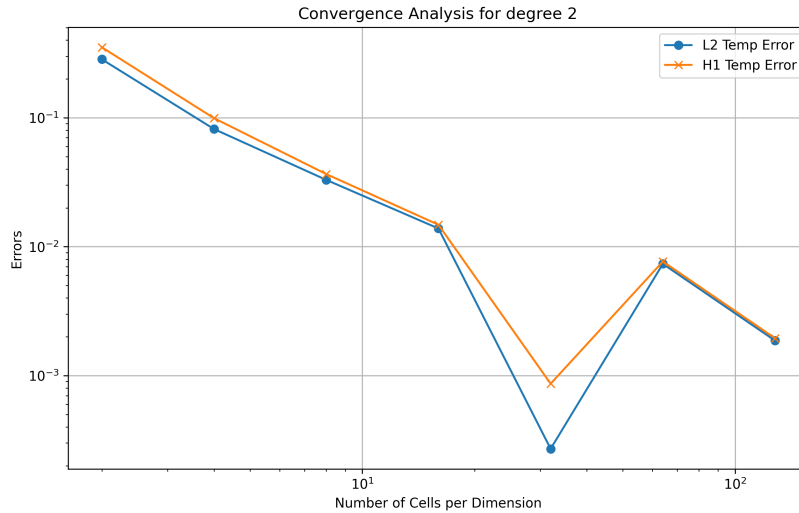


Figure 3.3: Error plot of the temperature field ( $\|T - T^h\|_{L^2(\Omega)}$  and  $\|T - T^h\|_{H^1(\Omega)}$ ) with  $d = 2$  B-splines and  $\text{lim} = 17.0$

In this figure, we can observe that the error in the temperature field is decreasing with the number of cells  $n_{cells}$  until  $n_{cells} = 32$ . After that, the error is increasing and decreases again. This behavior is likely due to the interaction between the mesh refinement, the B-spline approximation properties and the properties of the medium. When the degree of the B-splines is set to 3, we can see notice in the figure 3.4, that the hollow moves to a lower number of cells.

The same phenomenon is observed for the displacement field. One reason that can explain this phenomenon is the placement of the B-spline knots and the corresponding basis functions. As the mesh is refined, the B-spline basis functions become more localized, which can lead to better

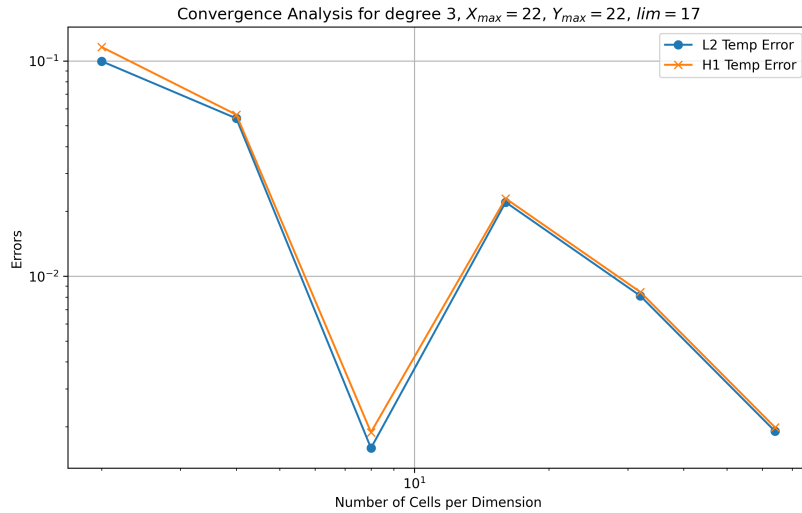
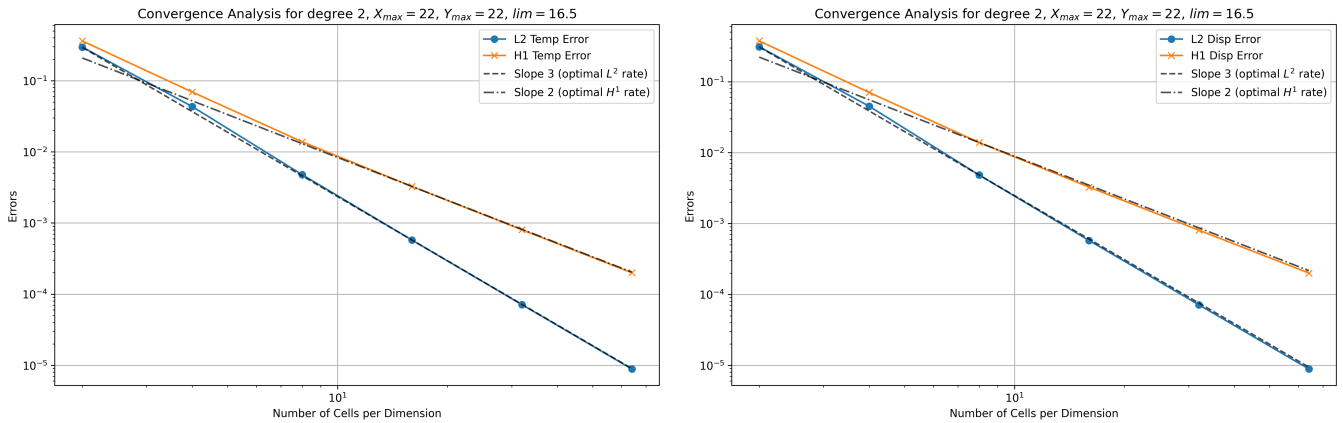


Figure 3.4: Error plot of the temperature field ( $\|T - T^h\|_{L^2(\Omega)}$  and  $\|T - T^h\|_{H^1(\Omega)}$ ) with  $d = 3$  B-splines and  $\text{lim} = 17.0$

approximation properties in certain regions of the domain. In the medium that we are considering, the line  $y = \text{lim} = 17.0$  plays a crucial role in the behavior of the solution because it corresponds to a significant change in the material properties. Moreover, PSYDAC cannot handle coefficients defined piecewise so it is necessary to approximate Heaviside functions to defined coefficients. For example,  $\lambda(y)$  is defined by:

$$\lambda(y) = \left( (\lambda_W - \lambda_{Cu}) \frac{x}{\text{lim}} + \lambda_{Cu} \right) H(\text{lim} - x) + \lambda_W H(x - \text{lim}) \quad H \text{ is the Heaviside function.}$$

One hypothesis that can be made to verify the role of the line  $y = \text{lim}$  is to move its value up and down and observe the effect on the solution. Especially, it's possible to move the value of  $\text{lim}$  to 16.5. This value corresponds to a line with breakpoints when the domain  $\Omega$  is discretized into different cells.



(a) Error plot of the temperature field

(b) Error plot of the displacement field

Figure 3.5: Error plots with  $\text{lim} = 16.5$  and degree 2 B-splines

In this case, we can observe the optimal convergence behavior of the error as predicted by the theory. So the position of the line  $y = \text{lim}$  is crucial for the accuracy of the solution and the simulation. To make the simulation possible in case described in subsection 3.2.1, we need to get a simulation setup that solves the problem when  $\text{lim} = 17$ . For the moment, the function which discretised the domain and create the finite dimensional spline space takes only the number of cells

per direction as argument. I have implemented a new feature to the library which allows the user to provide a custom discretisation grid. This feature required to add new functions to the `Geometry` class and modify the previous `discretize` function in PSYDAC. To ensure the correct working of this new feature, I have also implemented a set of unit tests. This new feature allows the user to define a

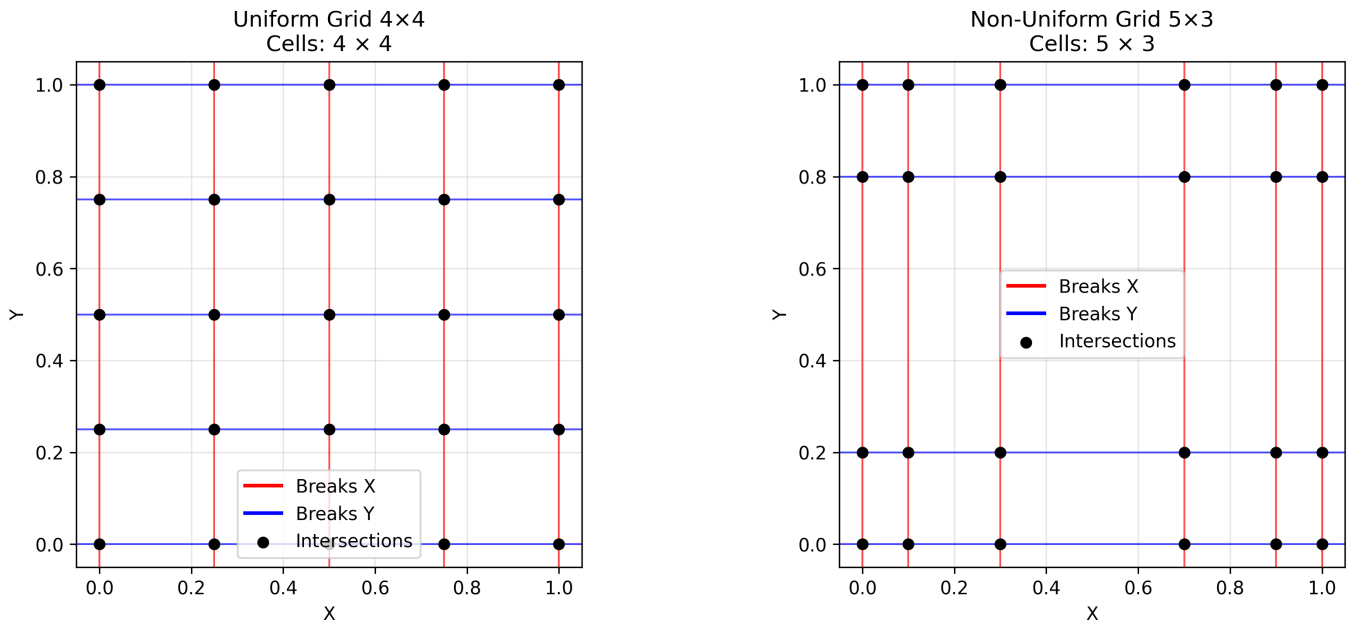


Figure 3.6: Example of a custom discretisation grid

custom grid for the discretisation of the domain. A entire description of this feature is available on GitHub : <https://github.com/pyccel/psydac/pull/518>

# Chapter 4

## References

- [EG04] Alexandre Ern and Jean-Luc Guermond. *Theory and Practice of Finite Elements*. en. Ed. by S. S. Antman, J. E. Marsden, and L. Sirovich. Vol. 159. Applied Mathematical Sciences. New York, NY: Springer New York, 2004. ISBN: 978-1-4419-1918-2 978-1-4757-4355-5. DOI: 10.1007/978-1-4757-4355-5. URL: <http://link.springer.com/10.1007/978-1-4757-4355-5> (visited on 06/16/2025).
- [Bof+08] Daniele Boffi et al. *Mixed Finite Elements, Compatibility Conditions, and Applications: Lectures given at the C.I.M.E. Summer School held in Cetraro, Italy June 26–July 1, 2006*. en. Ed. by Daniele Boffi et al. Vol. 1939. Lecture Notes in Mathematics. Berlin, Heidelberg: Springer Berlin Heidelberg, 2008. ISBN: 978-3-540-78314-5 978-3-540-78319-0. DOI: 10.1007/978-3-540-78319-0. URL: <http://link.springer.com/10.1007/978-3-540-78319-0> (visited on 06/16/2025).
- [BS08] Susanne C. Brenner and L. Ridgway Scott. *The Mathematical Theory of Finite Element Methods*. en. Ed. by J. E. Marsden, L. Sirovich, and S. S. Antman. Vol. 15. Texts in Applied Mathematics. New York, NY: Springer New York, 2008. ISBN: 978-0-387-75933-3 978-0-387-75934-0. DOI: 10.1007/978-0-387-75934-0. URL: <http://link.springer.com/10.1007/978-0-387-75934-0>.
- [Gou13] Phillip L. Gould. *Introduction to Linear Elasticity*. en. New York, NY: Springer New York, 2013. ISBN: 978-1-4614-4832-7 978-1-4614-4833-4. DOI: 10.1007/978-1-4614-4833-4. URL: <https://link.springer.com/10.1007/978-1-4614-4833-4>.
- [DV+14] L. Beirão Da Veiga et al. “Mathematical analysis of variational isogeometric methods”. en. In: *Acta Numerica* 23 (May 2014), pp. 157–287. ISSN: 0962-4929, 1474-0508. DOI: 10.1017/S096249291400004X. URL: [https://www.cambridge.org/core/product/identifier/S096249291400004X/type/journal\\_article](https://www.cambridge.org/core/product/identifier/S096249291400004X/type/journal_article) (visited on 06/26/2025).
- [MS15] Arnd Meyer and Rolf Springer. *Basics of Linear Thermoelasticity*. English. Preprint 15-03. First published on 06.02.2015. Technische Universität Chemnitz, 2015. URL: <https://nbn-resolving.org/urn:nbn:de:bsz:ch1-qucosa-160178>.
- [Per16] Anna Persson. “A generalized finite element method for linear thermoelasticity”. English. Licentiate Thesis. Gothenburg, Sweden: Chalmers University of Technology and University of Gothenburg, 2016.
- [Cin18] Emma Cinatl. “Finite Element Discretizations for Linear Elasticity”. en. PhD thesis. Clemson University, 2018.
- [GHR22] Y. Güclü, S. Hadjout, and A. Ratnani. “PSYDAC: a high-performance IGA library in Python”. en. In: *8th European Congress on Computational Methods in Applied Sciences and Engineering*. CIMNE, 2022. DOI: 10.23967/eccomas.2022.227. URL: [https://www.scipedia.com/public/Guclu\\_et\\_al\\_2022a](https://www.scipedia.com/public/Guclu_et_al_2022a) (visited on 06/17/2025).

[Che24] Long Chen. “Variational Formulation of linear elasticity”. en. In: (2024).

# Chapter 5

## Appendices

### 5.1 Other plots of solutions for the problem with Dirichlet Homogeneous Boundary Conditions